

# FedMPDD: Communication-Efficient Federated Learning with Privacy Preservation Attributes via Projected Directional Derivative

Mohammadreza Rostami and Solmaz S. Kia, *Senior Member, IEEE*

**Abstract**—This paper introduces FedMPDD (Federated Learning via Multi-Projected Directional Derivatives), a novel algorithm that simultaneously optimizes bandwidth utilization and enhances privacy in Federated Learning. The core idea of FedMPDD is to encode each client’s high-dimensional gradient by computing its directional derivatives along multiple random vectors. This compresses the gradient into a much smaller message, significantly reducing uplink communication costs from  $\mathcal{O}(d)$  to  $\mathcal{O}(m)$ , where  $m \ll d$ . The server then decodes the aggregated information by projecting it back onto the same random vectors. Our key insight is that averaging multiple projections overcomes the dimension-dependent convergence limitations of a single projection. We provide a rigorous theoretical analysis, establishing that FedMPDD converges at a rate of  $\mathcal{O}(1/\sqrt{K})$ , matching the performance of FedSGD. Furthermore, we demonstrate that our method provides some inherent privacy against gradient inversion attacks due to the geometric properties of low-rank projections, offering a tunable privacy-utility trade-off controlled by the number of projections. Extensive experiments on benchmark datasets validate our theory and demonstrates our results.

## I. INTRODUCTION

Federated Learning (FL) is a foundational paradigm for collaboratively training models across  $N$  edge devices by leveraging their local computational resources [1]–[3]. Beyond traditional machine learning applications, FL has been extended to control systems, including model-free learning with heterogeneous dynamical systems [4] and federated linear quadratic regulator approaches [5]. FL seeks to solve the distributed optimization problem

$$\text{minimize}_{\mathbf{x} \in \mathbb{R}^d} \quad f(\mathbf{x}) = \frac{1}{N} \sum_{i=1}^N f_i(\mathbf{x}), \quad (1)$$

where  $f_i : \mathbb{R}^d \rightarrow \mathbb{R}$  is the local objective (loss) function of client  $i$ , and  $f : \mathbb{R}^d \rightarrow \mathbb{R}$  is the global objective. Lacking central access to local objectives, FL iteratively communicates between a server and a client subset  $\mathcal{A}_k$  ( $|\mathcal{A}_k| = \beta N$ , where  $\beta \in (0, 1]$  denotes the client participation rate). In each round  $k$ , the server sends out the global model  $\mathbf{x}_k$ . Selected clients compute local updates (e.g., mini-batch gradients  $\mathbf{g}_i(\mathbf{x}_k)$ ) and transmit them to the server. The server aggregates these gradients by averaging:  $\mathbf{g}(\mathbf{x}_k) = \frac{1}{\beta N} \sum_{i \in \mathcal{A}_k} \mathbf{g}_i(\mathbf{x}_k)$ , and updates the global model:  $\mathbf{x}_{k+1} = \mathbf{x}_k - \eta \mathbf{g}(\mathbf{x}_k)$ , as in FedSGD [1], where  $\eta$  is a suitable learning rate.

A key bottleneck in FL algorithms like FedSGD is the substantial uplink communication overhead from transmitting  $d$

dimensional gradients  $\mathbf{g}_i(\mathbf{x}_k)$  from clients to the server, requiring  $32d$  bits per client per round, assuming single-precision floating-point representation (32 bits per value). For instance, a ResNet-18 model ( $\sim 11 \times 10^6$  parameters) necessitates approximately 42MB transmission per client per round. This high cost severely impacts efficiency in bandwidth-constrained real-world deployments [6]–[10]. Strategies to reduce FL communication volume or frequency fall into three main classes: *model compression*, *local computation with client selection*, and *gradient compression*. Model compression reduces global model size, for example, by using smaller models with local representations [11]. Local computation and client selection decrease communication frequency or the number of clients per round through techniques like multiple local updates [1], [12], [13] and client subset selection [11], [14]. Gradient compression reduces the size of transmitted gradients using methods like quantization [15]–[21], sparsification [22], [23], and structured/sketched updates. Structured updates, such as low-rank adaptation [24]–[30], use a pre-defined subspace for parameters, while sketched updates compress gradients using a shared random matrix fixed at initialization via techniques like projection matrices [31]–[33] or Count-Sketch [22], [34]–[36]. These approaches rely on a *static* projection for all clients and rounds. While these existing methods provide varying degrees of communication reduction, they often face trade-offs between compression ratio, computational overhead, convergence guarantees, and adaptability to different communication budgets, motivating the need for fundamentally new paradigms that can achieve more aggressive communication reduction without sacrificing convergence performance.

This paper proposes FedMPDD (Federated learning with Multi-Projected Directional Derivatives), a novel framework that fundamentally tackles the critical communication efficiency bottleneck to enable more practical and scalable deployment of FL in bandwidth-constrained environments. Unlike existing gradient compression techniques, our approach introduces a fundamentally new multiplicative encoding paradigm through the *projected directional derivative*—a concept recently explored in optimization contexts including balancing computational cost and memory in deep learning gradient calculations [37]–[41] and zeroth-order optimization [42]. The method we propose follows the core structure of FedSGD but achieves dramatic communication reduction by employing the *projected directional derivative*  $\hat{\mathbf{g}}_i(\mathbf{x}_k) = \mathbf{u}_{k,i}^\top \mathbf{g}_i(\mathbf{x}_k) \mathbf{u}_{k,i}$  (defined in (1)) instead of the full stochastic gradient  $\mathbf{g}_i(\mathbf{x}_k)$ . We decompose this projected directional gradient into a scalar directional derivative  $\mathbf{u}_{k,i}^\top \mathbf{g}_i(\mathbf{x}_k)$  computed locally by client  $i$ . Each client independently samples  $\mathbf{u}_{k,i}$ , then transmits

The authors are with the Department of Mechanical and Aerospace Engineering, University of California Irvine, Irvine, CA 92697, {mrostam2, solmaz}@uci.edu.

only two scalars: the directional derivative  $\mathbf{u}_{k,i}^\top \mathbf{g}_i(\mathbf{x}_k)$  and the random seed  $r_{k,i}$  used to generate  $\mathbf{u}_{k,i}$ . On the server side, the received seed  $r_{k,i}$  is used to reconstruct the identical  $d$ -dimensional vector  $\mathbf{u}_{k,i}$ , enabling the server to form the gradient estimator  $\hat{\mathbf{g}}_i(\mathbf{x}_k)$  without ever transmitting the full vector. However, our analysis shows that the noisy gradient estimator from a single projected directional derivative would severely degrade performance. To address this, we propose our main algorithm FedMPDD, which introduces a principled multi-projection aggregation mechanism that averages  $m$  projected directional derivatives. Crucially, unlike structured and sketched updates that rely on static projections, our approach uses a *dynamic* projection strategy where the projection directions  $\mathbf{u}_{k,i}$  are randomly and independently sampled for each client  $i$  at every round  $k$ . We show that when  $m$  independent projections are aggregated, the classical Johnson–Lindenstrauss guarantees (see details in Section III) ensure that the gradient norm is preserved up to small distortion with high probability. As a result, FedMPDD achieves accurate and stable gradient approximation by transmitting only  $m+1$  scalars per client per round reducing communication from  $32d$  to  $32(m+1)$  bits and achieving orders of magnitude savings (e.g., from 42MB to kilobytes for ResNet-18) while maintaining  $\mathcal{O}(1/\sqrt{K})$  convergence rates comparable to full-gradient methods.

While our primary focus is communication efficiency, an interesting emergent property of our encoding scheme is that it naturally provides some level of privacy protection. In FL implementations, Gradient Inversion Attacks (GIAs) [43]–[48] (detailed in Appendix A) remain a critical security concern, where a curious server can reconstruct raw data from transmitted gradients. Conventional defenses, such as Local Differential Privacy (LDP) [49]–[52], rely on injecting noise, which introduces a known trade-off between privacy guarantee and model convergence [53]. Other schemes have combined differential privacy with gradient compression [54]–[57], typically through adding Gaussian noise before quantization or integrating DP into quantization schemes, though these approaches often assume a trusted server and introduce convergence-degrading noise. In contrast, the privacy preservation in FedMPDD arises inherently from the geometric properties of our communication reduction mechanism. Specifically, the encoding matrix  $\mathbf{u}_{k,i} \mathbf{u}_{k,i}^\top$  is rank-deficient ( $\text{rank} = 1 \ll d$ ), which creates an underdetermined system when attempting to invert the gradient. This nullspace property prevents unique gradient recovery, offering a privacy defense against GIAs that is fundamentally different from additive noise methods and is achieved without sacrificing the communication benefits.

The key contributions of this work are summarized as follows:  
leftmargin=10pt

- Significant Communication Reduction: FedMPDD dramatically reduces uplink communication from  $\mathcal{O}(d)$  to just  $m+1$  scalars per client per round ( $\mathcal{O}(m)$  bits, where  $m \ll d$ ).
- Fast Convergence with Multi-Projection Averaging: Through our novel multi-projection averaging mechanism with dynamic projections, FedMPDD achieves a conver-

gence rate of  $\mathcal{O}(1/\sqrt{K})$  (Theorem 2), comparable to the uncompressed FedSGD baseline. The parameter  $m$  provides a tunable trade-off between communication cost and convergence speed.

- Inherent Privacy Preservation: As a natural by-product of our rank-deficient communication scheme, FedMPDD provides an inherent defense against GIA attacks without the need for convergence-degrading noise injection.

The remainder of this paper is organized as follows. Section II introduces the projected directional derivative, provides the motivation behind the proposed approach, and describes a naive implementation of the proposed mechanism and its challenges. Section III then presents the FedMPDD algorithm, details its update steps, and develops the convergence analysis, including convergence rates and privacy-preservation properties. Section IV reports numerical experiments, and Section V concludes the paper. For brevity, all proofs and supplementary experimental results are presented in the appendices.

## II. FL VIA PROJECTED DIRECTIONAL DERIVATIVES

The *projected directional derivative* is formally defined as:

**Definition 1 (projected directional derivative):** For a differentiable function  $f : \mathbb{R}^d \rightarrow \mathbb{R}$  the *projected directional derivative* is  $\widehat{\nabla f}(\mathbf{x}) := (\mathbf{u}^\top \nabla f(\mathbf{x})) \mathbf{u}$ , where  $\nabla f(\mathbf{x})$  is the gradient of  $f$  and  $\mathbf{u} \in \mathbb{R}^d$  is a random perturbation vector with entries  $u_i$  that are independently and identically distributed (i.i.d.) with zero mean and unit variance.  $\square$

The projected directional derivative satisfies  $\widehat{\nabla f}(\mathbf{x})^\top \nabla f(\mathbf{x}) \geq 0$  and  $\mathbb{E}[\widehat{\nabla f}(\mathbf{x})] = \nabla f(\mathbf{x})$  (unbiased estimator for gradient) and thus makes  $\mathbf{x}_{k+1} = \mathbf{x}_k - \eta \widehat{\nabla f}(\mathbf{x})$  to behave as a iterative successive descent (i.e.,  $\mathbb{E}[f(\mathbf{x}_{k+1})|\mathbf{x}_k] \approx f(\mathbf{x}_k) - \eta \|\nabla f(\mathbf{x})\|^2 < f(\mathbf{x}_k)$  for small  $\eta > 0$ ). This stands in contrast to structured/sketched updates, whose gradient estimator  $\widehat{\nabla f}(\mathbf{x})$  is often biased ( $\mathbb{E}[\widehat{\nabla f}(\mathbf{x})] \neq \nabla f(\mathbf{x})$ ) and can violate the descent condition, thus lacking a general guarantee of progress.

Within the framework of FedSGD, we consider an implementation that instead of the stochastic gradient  $\mathbf{g}(\mathbf{x}_k)$ , we employ the *projected directional derivative*  $\hat{\mathbf{g}}(\mathbf{x}_k)$  defined as:

$$\begin{aligned} \hat{\mathbf{g}}(\mathbf{x}_k) &= \frac{1}{\beta N} \left( \sum_{i \in \mathcal{A}_k} \underbrace{\mathbf{u}_{k,i}^\top \mathbf{g}_i(\mathbf{x}_k)}_{s_i^k: \text{client upload}} \underbrace{\mathbf{u}_{k,i}}_{\text{server-side projection}} \right) \\ &= \frac{1}{\beta N} \sum_{i \in \mathcal{A}_k} s_i^k \mathbf{u}_{k,i}. \end{aligned} \quad (2)$$

Considering the decomposition shown in (2), we propose FedPDD, presented in Algorithm 1, that proceeds as follows: each iteration begins with the server broadcasting the current model  $\mathbf{x}_k \in \mathbb{R}^d$  to a sampled client set  $\mathcal{A}_k$  (line 4). Upon receipt, each client generates a local random vector  $\mathbf{u}_{k,i}$  using its private seed  $r_{k,i}$  (line 6). The client encodes its local stochastic gradient into a scalar  $s_{k,i}$  using the directional derivative along  $\mathbf{u}_{k,i}$ , and uploads this scalar together with the seed  $r_{k,i}$ , which is essential for enabling convergence (line 9). The server aggregates and decodes these scalars to update the global model  $\mathbf{x}_{k+1}$  (lines 12-17). The design of FedPDD

**Algorithm 1** FedPDD: Federated Learning via Projected Directional Derivative

---

```

1: Input:  $\mathbf{x}_0 \in \mathbb{R}^d$ , learning rate  $\eta$ , rounds  $K$ , client fraction  $\beta \in (0, 1]$ 
2: for each round  $k = 0, 1, \dots, K - 1$  do
3:   Server samples client set  $\mathcal{A}_k$  with size  $\beta N$ 
4:   Server broadcasts  $\mathbf{x}_k$  to all  $i \in \mathcal{A}$ 
5:   for each client  $i \in \mathcal{A}_k$  in parallel do
6:     Generate i.i.d. Rademacher vector  $\mathbf{u}_k \in \{-1, +1\}^d$  using seed
       $r_{k,i}$ 
7:     Compute local stochastic gradient  $\mathbf{g}_i(\mathbf{x}_k)$ 
8:     Encode:  $s_i^k = \mathbf{u}_{k,i}^\top \mathbf{g}_i(\mathbf{x}_k)$ 
9:     Upload  $s_i^k \in \mathbb{R}$  and  $r_{k,i} \in \mathbb{R}$  to the server
10:    end for
11:     $\Delta_{\text{sum}} \leftarrow \mathbf{0}_d$                                  $\triangleright$  reset the estimator
12:    for each client  $i \in \mathcal{A}_k$  do                          $\triangleright$  on the server side
13:      Server generates Rademacher vector  $\mathbf{u}_{k,i} \in \{-1, +1\}^d$  using
        seed  $r_{k,i}$ 
14:      Decode:  $\Delta_{\text{sum}} \leftarrow \Delta_{\text{sum}} + s_i^k \mathbf{u}_{k,i}$ 
15:    end for
16:    Aggregate:  $\hat{\mathbf{g}}(\mathbf{x}_k) = \frac{1}{\beta N} \Delta_{\text{sum}}$ 
17:    Model update:  $\mathbf{x}_{k+1} = \mathbf{x}_k - \eta \hat{\mathbf{g}}(\mathbf{x}_k)$ 
18:  end for
19: Output:  $\mathbf{x}_K$ 

```

---

incorporates two key strategic choices. First, it employs a scalar seed  $r_{k,i}$  to generate the identical  $d$ -dimensional vector  $\mathbf{u}_{k,i}$  on the server side, thereby eliminating the need to transmit  $\mathbf{u}_{k,i}$  directly while still ensuring convergence. Second, although any zero-mean, unit-variance distribution for  $\mathbf{u}_{k,i}$  guarantees an unbiased projected directional derivative, our strategic choice of the Rademacher distribution for generating  $\mathbf{u}_{k,i}$  yields lower variance compared to the standard normal distribution as established in the result below.

**Lemma 1** (Variance Reduction via Distribution Choice; proof in Appendix B): *Consider the projected directional stochastic gradient  $\hat{\mathbf{g}}(\mathbf{x}) = \mathbf{u}^\top \mathbf{g}(\mathbf{x})\mathbf{u}$ , where the random direction  $\mathbf{u} \in \mathbb{R}^d$  is drawn from either (i) the standard normal distribution  $\mathcal{N}(\mathbf{0}, \mathbf{I}_d)$ , or (ii) the Rademacher distribution with i.i.d. entries in  $\{-1, +1\}$  (i.e.,  $\mathbb{P}(u_j = \pm 1) = \frac{1}{2}$  for all  $j = 1, \dots, d$ ). The difference in variance between these two choices satisfies:*

$$\text{Var}_{\mathbf{u} \sim \mathcal{N}(\mathbf{0}, \mathbf{I}_d)} [\hat{\mathbf{g}}(\mathbf{x})] - \text{Var}_{\mathbf{u} \sim \text{Rademacher}^d} [\hat{\mathbf{g}}(\mathbf{x})] = 2 \|\mathbf{g}(\mathbf{x})\|^2 \mathbf{I}_d,$$

where  $\mathbf{g}(\mathbf{x})$  is the true stochastic gradient.  $\square$

The preliminary FedPDD algorithm offers two appealing properties. First, it provides significant communication reduction, as clients only transmit two scalars instead of a full gradient vector. Second, it ensures intrinsic privacy preservation due to the rank-deficient nature of the single-vector projection:

$$\underbrace{\hat{\mathbf{g}}_i(\mathbf{x}_k)}_{\text{Known}} = (\mathbf{u}_{k,i}^\top \mathbf{g}_i(\mathbf{x}_k)) \mathbf{u}_{k,i} = \underbrace{(\mathbf{u}_{k,i} \mathbf{u}_{k,i}^\top)}_{\text{Known, Rank-1 Matrix}} \mathbf{g}_i(\mathbf{x}_k). \quad (3)$$

Since  $\mathbf{u}_{k,i} \mathbf{u}_{k,i}^\top$  is a rank-1 matrix with a  $(d - 1)$ -dimensional nullspace (by Sylvester's theorem [58]), equation (3) does not admit a unique solution: any  $\mathbf{g}_i(\mathbf{x}_k) + \mathbf{v}$  with  $\mathbf{v} \in \ker(\mathbf{u}_{k,i} \mathbf{u}_{k,i}^\top)$  also satisfies the equation. This large nullspace inherently introduces substantial uncertainty, making it impossible to uniquely reconstruct the true local gradient (see Section III-A for further discussion). However, as the re-

sult below shows, these benefits are offset by poor convergence performance. To analyze the convergence behavior of FedPDD, we first introduce some widely used conventional assumptions [59]–[61] on the cost function, similar to those used in the analysis of FedSGD.

**Assumption 1** (Regularity Conditions on Local Objectives): For each client  $i$ , the local function  $f_i$  is  $L$ -smooth, i.e., for all  $\mathbf{x}, \mathbf{y} \in \mathbb{R}^d$ ,  $\|\nabla f_i(\mathbf{x}) - \nabla f_i(\mathbf{y})\| \leq L \|\mathbf{x} - \mathbf{y}\|$ . In addition, the stochastic gradient is bounded in second moment:  $\mathbb{E}[\|\mathbf{g}_i(\mathbf{x})\|^2] \leq G^2$  for all  $\mathbf{x} \in \mathbb{R}^d$ , and the variance of local gradients relative to the global gradient is bounded:  $\frac{1}{N} \sum_{i=1}^N \|\nabla f_i(\mathbf{x}) - \nabla f(\mathbf{x})\|^2 \leq \sigma^2$ .  $\square$

**Theorem 1** (Convergence Bound of FedPDD Algorithm): *Consider FedPDD algorithm with a step size  $\eta = \frac{1}{L\sqrt{K}}$ , and suppose that Assumption 1 holds. Then, FedPDD algorithm converges to a stationary point of problem (1) at a rate of  $\mathcal{O}(d/\sqrt{K})$ , satisfying the following upper bound*

$$\frac{1}{K} \sum_{k=0}^{K-1} \mathbb{E} [\|\nabla f(\mathbf{x}_k)\|^2] \leq \underbrace{\mathcal{O}\left(\frac{L(f(\mathbf{x}_0) - f^*)}{\sqrt{K}}\right)}_{\text{due to initialization}} + \underbrace{\mathcal{O}\left(\frac{\sigma^2(1/\beta - 1)}{K\sqrt{K}}\right)}_{\text{due to client sampling}} + \underbrace{\mathcal{O}\left(\frac{dG^2}{\sqrt{K}}\right)}_{\text{due to projected directional derivative}}, \quad (4)$$

where  $\beta \in (0, 1]$  denotes the client participation fraction, and  $f^*$  denotes the global minimum of  $f$ .  $\square$

The third term in the convergence bound (4) stems from the rank-1 projection operator  $\mathbf{u}_{k,i} \mathbf{u}_{k,i}^\top$  (proof in Appendix B). Despite the projected directional derivative being an unbiased estimator, this rank-one map introduces high variance due to a magnitude scaling of  $\sqrt{d}$  compared to the gradient:

$$\begin{aligned} \mathbb{E}_{\mathbf{u}} [\|\hat{\mathbf{g}}_i(\mathbf{x}_k)\|] &\leq \sqrt{\mathbb{E}_{\mathbf{u}} [\|\hat{\mathbf{g}}_i(\mathbf{x}_k)\|^2]} \\ &= \sqrt{d \|\mathbf{g}_i(\mathbf{x}_k)\|^2} = \sqrt{d} \|\mathbf{g}_i(\mathbf{x}_k)\|. \end{aligned}$$

The uncontrollable  $\sqrt{d}$  scaling yields the  $\mathcal{O}(d/\sqrt{K})$  convergence rate highlighted in (4), which scales poorly with model dimension  $d$ . Consequently, FedPDD requires roughly  $d$  times more iterations than FedSGD ( $\mathcal{O}(1/\sqrt{K})$  rate) to achieve comparable performance, resulting in total uplink communication of  $\mathcal{O}(d/\sqrt{K} \times \beta N)$  bits asymptotically matching FedSGD's cost and negating the per-round savings. While adjusting the step size to  $\eta = \frac{1}{dL\sqrt{K}}$  could mitigate the  $d$  factor in the projection-induced term, it necessitates a smaller overall step size that significantly slows convergence by amplifying the influence of the other terms in (4). The larger variance also causes potential overshooting in the FedPDD updates. These critical limitations motivate the development of FedMPDD in Section III and Algorithm 2, which addresses these shortcomings through a multi-projection approach for practical large-scale problems.

### III. FL VIA MULTI-PROJECTED DIRECTIONAL DERIVATIVES

To address the limitation of FedPDD, we extend the estimator by sampling multiple directions. Specifically, at iteration  $k$ ,

each selected client  $i$  draws  $m$  i.i.d. Rademacher vectors  $\{\mathbf{u}_{k,i}^{(j)}\}_{j=1}^m \subset \{-1, +1\}^d$ . To better understand the mechanism, we now stack the sampled vectors as columns to form the matrix  $\mathbf{U}_{k,i} \in \mathbb{R}^{d \times m}$ . Using this construction, the generalized estimator is defined as:

$$\hat{\mathbf{g}}_i(\mathbf{x}_k) := \frac{1}{m} \sum_{j=1}^m (\mathbf{u}_{k,i}^{(j)\top} \mathbf{g}_i(\mathbf{x}_k)) \mathbf{u}_{k,i}^{(j)} = \frac{1}{m} \mathbf{U}_{k,i} \left( \mathbf{U}_{k,i}^\top \mathbf{g}_i(\mathbf{x}_k) \right),$$

$$\mathbf{U}_{k,i} = \begin{bmatrix} \mathbf{u}_{k,i}^{(1)} & \mathbf{u}_{k,i}^{(2)} & \cdots & \mathbf{u}_{k,i}^{(m)} \end{bmatrix} \in \mathbb{R}^{d \times m}. \quad (5)$$

As  $\mathbb{E}[\mathbf{U}_{k,i} \mathbf{U}_{k,i}^\top] = m \mathbf{I}_d$ , the estimator remains unbiased:  $\mathbb{E}[\hat{\mathbf{g}}_i(\mathbf{x}_k)] = \frac{1}{m} \mathbb{E}[\mathbf{U}_{k,i} \mathbf{U}_{k,i}^\top] \mathbf{g}_i(\mathbf{x}_k) = \mathbf{g}_i(\mathbf{x}_k)$ .

By constructing, the mapping  $\frac{1}{m} \mathbf{U}_{k,i} \mathbf{U}_{k,i}^\top$  satisfies the high-probability operator-norm Johnson–Lindenstrauss (JL) Lemma [62].

**Lemma 2** (JL Bound for Multi-Projected Directional Derivatives): *For any  $0 < \varepsilon < 1$  and  $0 < \delta < 1$ , if the number of sampled random directions satisfies*

$$m = \mathcal{O}\left(\frac{\ln(d/\delta)}{\varepsilon^2}\right), \quad (6)$$

*then with probability at least  $1 - \delta$ , the following bound holds:*

$$\left\| \frac{1}{m} \mathbf{U}_{k,i} (\mathbf{U}_{k,i}^\top \mathbf{g}_i(\mathbf{x}_k)) \right\| \leq (1 + \varepsilon) \|\mathbf{g}_i(\mathbf{x}_k)\|, \quad (7)$$

where  $\mathbf{U}_{k,i}$  is defined in (5) and its columns are sampled independently according to the projection direction distribution in Definition 1.  $\square$

The proof of this lemma follows trivially from the JL Lemma [62, Theorem 5.3]. This result implies that the mapping operator  $\frac{1}{m} \mathbf{U}_{k,i} \mathbf{U}_{k,i}^\top$  approximately preserves the norm of the client’s gradient with high probability, provided a sufficient number of sampled directions. Moreover, as  $m \rightarrow \infty$ , the mapping approaches the identity operator  $\frac{1}{m} \mathbf{U}_{k,i} \mathbf{U}_{k,i}^\top \rightarrow \mathbf{I}_d$  in expectation, due to the unbiasedness of the projection. Motivated by this probabilistic guarantee, which grows only logarithmically with the ambient dimension  $d$ , we design FedMPDD algorithm, presented in Algorithm 2, as a generalization of FedPDD algorithm. The following result provides a convergence guarantee for FedMPDD.

**Theorem 2** (Convergence Bound of FedMPDD Algorithm): *Let the step size  $\eta = \frac{1}{L\sqrt{K}}$ , and suppose that Assumption 1 holds. Let number of random vectors be  $m = O\left(\frac{\ln(d/\delta)}{\varepsilon^2}\right)$ . Then, FedMPDD algorithm converges to a stationary point of problem (1) at a rate of  $\mathcal{O}(1/\sqrt{K})$ , satisfying the following upper bound with probability at least  $1 - \delta$ ,*

$$\frac{1}{K} \sum_{k=0}^{K-1} \mathbb{E} \left[ \|\nabla f(\mathbf{x}_k)\|^2 \right] \leq \underbrace{\mathcal{O}\left(\frac{L(f(\mathbf{x}_0) - f^*)}{\sqrt{K}}\right)}_{\text{due to initialization}} +$$

$$\underbrace{\mathcal{O}\left(\frac{\sigma^2(1/\beta - 1)}{K\sqrt{K}}\right)}_{\text{due to client sampling}} + \underbrace{\mathcal{O}\left(\frac{\epsilon G^2}{\sqrt{K}}\right)}_{\text{due to Multi-projected directional derivatives}}, \quad (8)$$

where  $0 < \epsilon < 1$  is the distortion parameter,  $\beta \in (0, 1]$  denotes the client participation fraction, and  $f^*$  denotes the global minimum of  $f$ .  $\square$

**Remark 1:** [Choice of  $m$ ,  $\varepsilon$ , and  $\delta$ ] The number of random

---

**Algorithm 2** FedMPDD: Federated Learning via Multi-Projected Directional Derivatives

---

```

1: Input:  $\mathbf{x}_0 \in \mathbb{R}^d$ , learning rate  $\eta$ , rounds  $K$ , # random directions  $m$ , client fraction  $\beta \in (0, 1]$ 
2: for  $k = 0, 1, \dots, K - 1$  do
3:   Server samples client set  $\mathcal{A}_k$  with  $|\mathcal{A}_k| = \beta N$ 
4:   Server broadcasts  $\mathbf{x}_k$  to all  $i \in \mathcal{A}_k$ 
5:   for each client  $i \in \mathcal{A}_k$  in parallel do
6:     Compute local stochastic gradient  $\mathbf{g}_i(\mathbf{x}_k)$ 
7:     for  $j = 1, \dots, m$  do ▷ loop over projected directions
8:       Client generates i.i.d. Rademacher vector  $\mathbf{u}_{k,i}^{(j)} \in \{-1, +1\}^d$  using seed  $r_{k,i}$  and index  $j$ 
9:       Encode:  $\mathbf{s}_i^k[j] \leftarrow (\mathbf{u}_{k,i}^{(j)\top} \mathbf{g}_i(\mathbf{x}_k))$ 
10:      end for
11:      Upload  $\mathbf{s}_i^k \in \mathbb{R}^m$  and  $r_{k,i} \in \mathbb{R}$  to the server
12:    end for
13:     $\Delta_{\text{sum}} \leftarrow \mathbf{0}_d$  ▷ reset the estimator
14:    for each client  $i \in \mathcal{A}_k$  do ▷ on the server side
15:      for  $j = 1, \dots, m$  do ▷ re-generate the same projected directions
16:        Server generates i.i.d. Rademacher vector  $\mathbf{u}_{k,i}^{(j)} \in \{-1, +1\}^d$  using seed  $r_{k,i}$  and index  $j$ 
17:        Decode:  $\Delta_{\text{sum}} \leftarrow \Delta_{\text{sum}} + \frac{\mathbf{s}_i^k[j]}{m} \mathbf{u}_{k,i}^{(j)}$ 
18:      end for
19:    end for
20:    Aggregate:  $\hat{\mathbf{g}}(\mathbf{x}_k) = \frac{1}{\beta N} \Delta_{\text{sum}}$ 
21:    Model update:  $\mathbf{x}_{k+1} = \mathbf{x}_k - \eta \hat{\mathbf{g}}(\mathbf{x}_k)$ 
22:  end for
23: Output:  $\mathbf{x}_K$ 

```

---

directions  $m$  is selected according to the JL embedding requirement in (6) where  $\varepsilon \in (0, 1)$  controls the distortion of the projected gradient and  $\delta \in (0, 1)$  is the failure probability. In our setting,  $\varepsilon$  directly appears in the convergence bound (8) of Theorem 2 through the term  $\mathcal{O}\left(\frac{\epsilon G^2}{\sqrt{K}}\right)$ , and therefore acts as an accuracy knob, while  $\delta$  determines the confidence level with which the JL property holds. In practice, we fix  $\delta$  to a small constant (e.g.,  $\delta \in [10^{-3}, 10^{-1}]$ ) to ensure high-probability guarantees, and select  $\varepsilon$  in a moderate distortion regime (e.g.,  $\varepsilon \in [0.05, 0.2]$ ). With these choices,  $m$  is then computed using the above scaling and treated as a communication–accuracy trade-off parameter. In our experiments, we set  $m$  to be a small fraction of the ambient dimension, specifically in the range  $m \in [0.2\%, 4\%] \times d$ , which lies well within the JL-valid regime predicted by theory. All experimental results are conducted within this regime, ensuring that the theoretical guarantees apply throughout training.  $\square$

**Remark 2** (Computational Cost of FedMPDD): The client-side encoding in FedMPDD has a computational cost of  $\mathcal{O}(dm)$  (see lines 7–10 of the FedMPDD algorithm; as reported in Table XIX for one representative experiment, this computational time is negligible and does not constitute a bottleneck in our experiments). While this may initially seem costly, it is often offset in practice, since in many federated learning settings, client models are deep neural networks and computing the full stochastic gradient (line 6) is already expensive. Recent work [38]–[40] has shown that computing the inner product  $\mathbf{u}^\top \mathbf{g}_i$  is significantly more efficient than computing the full gradient  $\mathbf{g}_i$ , because the operation can be implemented as a Jacobian–vector product (JVP), which leverages efficient vector–matrix multiplication in deep networks. Specifically, projected-forward methods reduce the time complexity of gradient computation from  $\mathcal{O}(h^2 p T^2)$  (for full forward-mode

autodiff) to  $\mathcal{O}(h^2T + hpT)$ , where  $h$ ,  $p$ , and  $T$  denote the hidden dimension, the number of parameters per layer, and the total number of layers, respectively. Motivated by these insights, FedMPDD can avoid computing  $\mathbf{g}_i$  explicitly (line 6) by fixing a single mini-batch  $\mathcal{B}_i^k$  and reusing it across all random directions. The encoding step (line 9) is then performed via the projected-forward approach using JVPs. We can show that when  $m < \frac{hpT}{h+p}$ , this strategy reduces overall client-side computation, making FedMPDD particularly suitable for resource-constrained devices. We empirically evaluate this strategy in our follow-up study (see Section IV).  $\square$

**Remark 3 (Communication Reduction and Efficiency in FedMPDD):** FedMPDD presented in Algorithm 2 significantly reduces per-round uplink communication by enabling clients to transmit only an  $m$ -dimensional vector  $\mathbf{s}_i^k \in \mathbb{R}^m$  together with a scalar seed number  $r_{k,i} \in \mathbb{R}$ , instead of the full  $d$ -dimensional gradient ( $m \ll d$ ). This is achieved by encoding the client's  $d$ -dimensional gradient through its projection onto a set of  $m$  random scalars (line 9). Moreover, the total communication cost over the full training horizon is reduced to  $\mathcal{O}(1/\sqrt{K} \times \beta N \times m)$ , where  $\beta$  is the client participation ratio and  $N$  is the number of clients. Since  $m$  grows only logarithmically with the problem dimension  $d$ , the communication savings become even more substantial for large-scale models. Our experiments such as one with model dimension  $d = 319,242$ , show that using only  $m = 600$  ( $\approx 0.2\%$  of  $d$ ) directions, FedMPDD matches the accuracy and convergence speed of baseline methods while substantially reducing uplink communication.  $\square$

### A. Privacy Preservation Attributes of FedMPDD

The privacy guarantees of FedMPDD are demonstrated under a standard honest-but-curious threat model.

**Definition 2 (Threat model):** An *honest-but-curious* adversary (e.g., the server) correctly follows the protocol but attempts to infer private client data by analyzing all accessible information, which includes communication messages, model architecture, and global hyperparameters.

Against this adversary, FedMPDD's privacy stems from its rank-deficient projection ( $m \ll d$ ), which creates quantifiable uncertainty for any party observing the transmitted data. We formalize this protection below.

**Lemma 3 (Gradient reconstruction error; proof in Appendix B):** For the reconstructed gradient estimator  $\hat{\mathbf{g}}_i(\mathbf{x}_k) = \frac{1}{m} \sum_{j=1}^m \mathbf{u}_{k,i}^{(j)} (\mathbf{u}_{k,i}^{(j)})^\top \mathbf{g}_i(\mathbf{x}_k)$ , the expected relative squared error is:

$$\mathbb{E}_{\mathbf{U}} [\|\hat{\mathbf{g}}_i(\mathbf{x}_k) - \mathbf{g}_i(\mathbf{x}_k)\|^2] / \|\mathbf{g}_i(\mathbf{x}_k)\|^2 = \frac{d-1}{m}. \quad (9)$$

$\square$

This inherent gradient ambiguity provides a formal defense against GIA attacks by establishing a lower bound on reconstruction error.

The following Lemma establishes a lower bound on the private data reconstruction error. We denote by  $(v, c)$  a private training

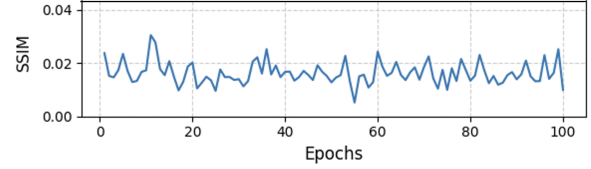


**Fig. 1:** SSIM scores from GIA [63] on LeNet using FedMPDD with  $m = 600$  remain consistently low (below 0.04) over 100 training epochs, demonstrating that privacy protection is independent of the training stage.

sample held by a client, where  $v$  represents the raw input data (e.g., an image) and  $c$  denotes the corresponding label.

**Lemma 4 (Lower bound on private data reconstruction error; proof in Appendix B):** Suppose an adversary attempts to reconstruct a private input vector  $v$  by minimizing  $\mathcal{L}(\hat{v}) := \|\frac{1}{m} \mathbf{U}_{k,i} \mathbf{U}_{k,i}^\top \mathbf{g}_i(v, c; \mathbf{x}_k) - \mathbf{g}_i(\hat{v}, c; \mathbf{x}_k)\|$ . The expected reconstruction error is lower bounded by:

$$\mathbb{E} [\|v - \hat{v}^*\|^2] \geq \frac{d-1}{m \cdot L_v(\mathbf{x})^2} \|\mathbf{g}_i(v, c; \mathbf{x}_k)\|^2, \quad (10)$$

where  $L_v(\mathbf{x})$  is the Lipschitz constant of the gradient with respect to  $v$ .  $\square$

Together, these lemmas establish that the gradient reconstruction error of  $\frac{d-1}{m}$  translates into a concrete lower bound on data recovery, creating a privacy barrier that scales with model dimension  $d$ .

Our approach offers some fundamental advantages over additive-noise methods. In FL with LDP, adding noise  $\zeta_i$  to each client's gradient yields a relative reconstruction error proportional to:

$$\begin{aligned} \text{Relative Reconstruction Error} &\propto \frac{\text{honest-but-curious}}{\|\mathbf{g}_i(\mathbf{x}_k)\|^2} \frac{\left\| \overbrace{\mathbf{g}_i(\mathbf{x}_k) + \zeta_i}^{\text{server observation}} - \mathbf{g}_i(\mathbf{x}_k) \right\|^2}{\|\mathbf{g}_i(\mathbf{x}_k)\|^2} \\ &= \frac{\mathbb{E}_{\zeta_i} [\|\zeta_i\|^2]}{\|\mathbf{g}_i(\mathbf{x}_k)\|^2} = \frac{d\tau^2}{\|\mathbf{g}_i(\mathbf{x}_k)\|^2}. \end{aligned} \quad (11)$$

where  $\tau^2$  is the variance of noise  $\zeta_i$ . This creates an inconsistency: large gradients are poorly protected, while small gradients can be overwhelmed by noise, potentially breaking convergence (when  $\|\zeta\| \gg \|\mathbf{g}\|$ , the perturbed gradient can flip the descent direction). Achieving consistent privacy with LDP requires large noise that degrades performance, and still incurs  $\mathcal{O}(d)$  communication cost. In contrast, FedMPDD provides a *consistent* relative reconstruction error of  $\frac{d-1}{m}$  that is independent of gradient magnitude. This design simultaneously ensures: (i) guaranteed descent direction ( $\mathbf{g}^\top \hat{\mathbf{g}} \geq 0$ ) without added noise, (ii) constant privacy through a fixed  $(d-m)$ -dimensional nullspace, and (iii) substantial communication savings ( $m \ll d$ ).

Our theoretical guarantees are supported by empirical results. Figure 2 illustrates FedMPDD's data obfuscation on CIFAR-10 for different values of  $m$ . Figure 1 shows that SSIM scores remain consistently low across training epochs, confirming that privacy protection is independent of gradient magnitude and training stage. However, a critical consideration remains when an adversary observes a client over multiple rounds. We formalize this concern below.

**Lemma 5 (Worst-Case Multi-Round Privacy Bound; proof in Appendix B):** Consider the worst-case scenario where the client's gra-

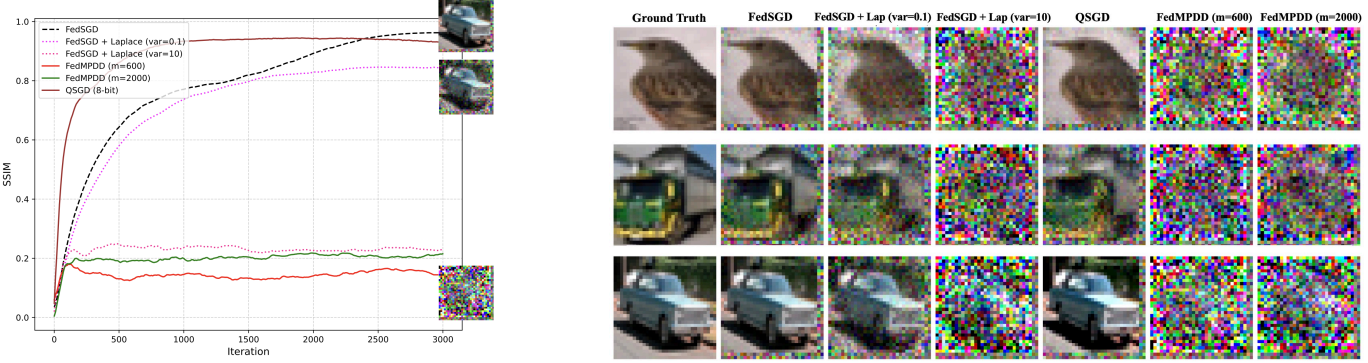


**Fig. 2:** GIA attack [63] visualization: SSIM scores (left) and reconstructed CIFAR-10 samples (right). LDP with small noise (columns 3–4) and QSGD (column 5) show significant data leakage, while FedMPDD (columns 6–7) demonstrates stronger privacy.

gradient  $g_i$  remains constant across all rounds. An adversary observing projections from  $T$  rounds obtains  $T \times m$  linear constraints on the  $d$ -dimensional gradient. Privacy is preserved (gradient cannot be uniquely recovered) as long as  $T < \frac{d}{m}$ .  $\square$

The bound  $T < \frac{d}{m}$  in this statement is due to the underdetermined system having a non-trivial nullspace of dimension  $d - T \times m > 0$ . This bound reflects an *observability constraint*: the adversary's rank- $m$  measurements per round are insufficient to reconstruct the full  $d$ -dimensional gradient. With typical settings ( $d \in [10^6, 10^9]$ ,  $m = 100$ ,  $T \in [10^2, 10^4]$ ), the condition  $T \times m < d$  is easily satisfied (e.g.,  $d = 10^6$  and  $m = 100$  allows  $T < 10^4$  rounds). Moreover, gradient evolution during training provides additional protection beyond this worst-case static analysis [64].

**Remark 4** (Privacy-communication trade-off): The parameter  $m$  serves as a tunable knob for the privacy-communication-accuracy trade-off. From a system-theoretic viewpoint,  $m$  controls the rank of the observation operator at each time step, regulating the observability of the client's gradient trajectory [65]. A larger  $m$  increases communication overhead (uplink message size scales with  $m$ ) and reduces privacy (more gradient information revealed), but improves gradient reconstruction accuracy, with expected error  $\frac{d-1}{m}$  (Lemmas 3 and 4). This fundamental trade-off where improving one aspect (e.g., accuracy) degrades another (e.g., privacy or communication efficiency) mirrors similar tensions in differential privacy. The worst-case bound  $T < d/m$  directly quantifies this: smaller  $m$  allows more training rounds while maintaining privacy, but may require more rounds to achieve convergence.  $\square$

Our experimental results across two attack families, including the recent GIA attacks [63] and the well-known deep leakage from gradients method [43] (details in Appendix A), support this theoretical finding and demonstrate that the predicted privacy protection holds in practice.

#### IV. NUMERICAL EXPERIMENTS

We conduct a comprehensive evaluation of the proposed algorithm against the baseline methods using multiple neural network architectures with varying parameter sizes: the LeNet model with  $d = 13,426$ , the CNN architecture from [66] with  $d = 61,706$ , and the CNN model from [1] with  $d = 319,242$ . Unless stated otherwise, data is partitioned among 100 clients; Tables I-II gives the model architectures of these benchmark models. Note that, MNIST and FASHIONMNIST datasets each contain 60,000 training samples and 10,000 test samples. The CIFAR-10 dataset consists of 50,000 training samples and 10,000 test samples. Moreover, under the non-i.i.d. data distribution, each client receives data from exactly two classes in the dataset. Experiments involving logistic regression are conducted on a MacBook Pro CPU. All other experiments are executed on an NVIDIA A100 GPU.

**TABLE I:** Model architecture of LeNet.

Layer	Type	Kernel Size	Output Shape	Activation
Input	-	-	$1 \times 28 \times 28$	-
Conv1	Conv2D	$5 \times 5$ , stride 2, padding 2	$12 \times 14 \times 14$	Sigmoid
Conv2	Conv2D	$5 \times 5$ , stride 2, padding 2	$12 \times 7 \times 7$	Sigmoid
Conv3	Conv2D	$5 \times 5$ , stride 1, padding 2	$12 \times 7 \times 7$	Sigmoid
Flatten	-	-	588	-
FC	Linear	-	10 (logits)	-

**TABLE II:** Model Architecture of CNN in [66].

Layer	Type	Kernel / Params	Output Shape	Activation
Input	-	-	$1 \times 28 \times 28$	-
Conv1	Conv2D	$5 \times 5$ , MaxPool(2)	$6 \times 12 \times 12$	ReLU
Conv2	Conv2D	$5 \times 5$ , MaxPool(2)	$16 \times 4 \times 4$	ReLU
Flatten	-	-	400	-
FC1	Linear	$400 \rightarrow 120$	120	ReLU
FC2	Linear	$120 \rightarrow 84$	84	ReLU
FC3	Linear	$84 \rightarrow 10$	10 (logits)	-

For a comprehensive evaluation, we tested client participation rates of 10%, 50%, and 100% across different tasks, considering both i.i.d. and non-i.i.d. data distributions (where each client accesses only a subset of classes in multi-class classification). Hyperparameter tuning details for each model are in Appendix C. For gradient inversion attacks, we employed two algorithms: (i) the recent method proposed by [63], and (ii) the well-known Deep Leakage from Gradients (DLG) algorithm [43], which reconstructs original input data (e.g., images) from shared gradients in distributed learning.

We compare the communication cost reduction of FedMPDD against a recent sketching-based method [66], a structured-based method [67], a top- $k$  sparsification method [68], and the quantization-based method QSGD [15]. For performance evaluation, FedSGD serves as the accuracy baseline. Our communication cost analysis includes total and per-round uplink overhead, as well as *i*) performance under a constrained communication budget and *ii*) the total communication cost to achieve target accuracy. To empirically validate FedMPDD's privacy enhancement against GIAs, we compare it to LDP with varying noise levels in image classification tasks.

To evaluate the quality of reconstructed images after the attack, we employ the Structural Similarity Index Measure (SSIM) [56], a widely used metric for assessing image similarity, where an SSIM value closer to 1 indicates a higher resemblance between the reconstructed image and the ground truth. For brevity, we only show a subset of the results and the full set of tables and training and accuracy curves are presented in Appendix D. Note that in our experiments, we did not fine-tune the value of  $m$  to explicitly optimize for the minimal communication cost and maximal privacy guarantees achievable by FedMPDD. Instead, we selected  $m = \mathcal{O}\left(\frac{\ln(d/\delta)}{\varepsilon^2}\right)$  for sufficiently small values of  $\delta$  and  $\varepsilon$ . In Table XVIII

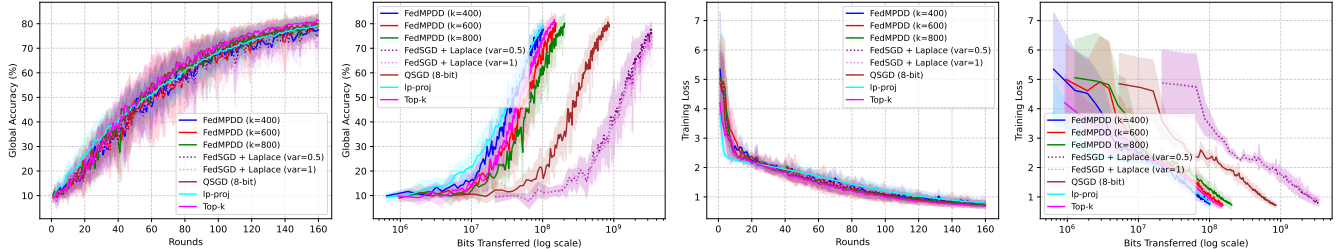


**Fig. 3:** Training loss and accuracy curves versus communication rounds and number of transmitted bits for the LeNet model on the MNIST dataset (i.i.d.).

**TABLE III:** Model Architecture of CNN in [1].

Layer	Type	Kernel / Params	Output Shape	Activation
Input	-	-	$3 \times 32 \times 32$	-
Conv1	Conv2D	$3 \times 3$	$128 \times 30 \times 30$	ReLU
	MaxPool	$2 \times 2$	$128 \times 15 \times 15$	-
Conv2	Conv2D	$3 \times 3$	$128 \times 13 \times 13$	ReLU
	MaxPool	$2 \times 2$	$128 \times 6 \times 6$	-
Conv3	Conv2D	$3 \times 3$	$128 \times 4 \times 4$	ReLU
Flatten	-	-	2048	-
FC1	Linear	$2048 \rightarrow 10$	10 (logits)	-

of Appendix D, we present experiments over a wide range of  $m$  values to further illustrate the findings of Theorem 2. As  $m$  becomes too small, both the rate of convergence and the accuracy deteriorate. Moreover, as we show in our reported results, the chosen values of  $m$  grow slightly with the parameter dimension  $d$  (ranging from a simple logistic model to a deep CNN model with over 300,000 parameters) while maintaining convergence performance comparable to FedSGD, making the proposed algorithm well-suited for large-scale problems. This empirical observation further supports the theoretical guarantees in Theorem 2, where  $m$  is required to grow logarithmically with the dimension  $d$  to retain the  $\mathcal{O}(1/\sqrt{K})$  convergence rate of FedSGD. Tables IV and V demonstrate FedMPDD’s effectiveness in reducing communication cost and its privacy preservation attribute. Our byte budget represents the *total uplink communication* permitted between active clients and the server across all training iterations, unlike per-round limits. We analyze the results from two complementary perspectives, beginning with those reported in Table V.

**Fixed budget (0.9 GB):** The objective here is to compare methods under a *fixed total uplink communication budget* of 0.9 GB, evaluating the maximum achievable test accuracy and the corresponding privacy leakage. In Table V FedSGD and its Laplace-noised variants rapidly exceed the communication budget in the very first iteration, making them impractical under realistic constraints. In contrast, FedMPDD stays well within the budget, achieving competitive accuracy thanks to its efficient projected directional derivative encoding. For example, with  $m = 600$  (0.2% of  $d$ ), FedMPDD reaches 40.8% test accuracy, significantly higher than QSGD (12.9%) and other baselines such as Ip-proj (34.7%) [66], Top-k (38.1%) [68], and SA-FedLora (35.8%) [67]. Importantly, although these baselines remain within the budget, they fail to provide consistent privacy guarantees, as their SSIM values (0.74 to 0.91) reveal substantial leakage under gradient inversion attacks. In contrast, FedMPDD achieves both stronger accuracy and substantially lower SSIM (0.14 to 0.22), highlighting its ability to simultaneously reduce communication and preserve privacy, rigorously established in Lemmas 3 and 4, arising from the  $(d - m)$ -dimensional nullspace of the multi-projected directional derivative.”

**Fixed accuracy (60% target):** Here, the objective is to compare methods based on the total uplink communication required to reach a fixed target test accuracy of 60%, while simultaneously evaluating privacy leakage. To achieve the same target accuracy, in Table V FedSGD and its noisy variants consume over 470 GB, exceeding the

budget by several orders of magnitude and leaking private information (SSIM  $> 0.8$ ). Similarly, QSGD requires more than 117 GB while still failing on privacy. Ip-proj, Top-k, and SA-FedLora are more communication-efficient, which is their primary goal, requiring only 1.8 to 2.3 GB, but they still exhibit weak privacy protection due to their high SSIM values. By contrast, FedMPDD with  $m = 600$  requires only 1.3 GB, representing a more than  $356\times$  reduction compared to FedSGD, and with  $m = 2000$ , it requires just 3.3 GB, still a  $144\times$  reduction. Crucially, FedMPDD attains these communication savings while keeping SSIM  $< 0.22$ , ensuring strong and constant privacy level.

Taken together, these results demonstrate that FedMPDD outperforms all baselines across both evaluation criteria: it matches or exceeds their communication efficiency while uniquely combining this with robust privacy protection. Competing methods (Ip-proj, Top-k, SA-FedLora) achieve communication reduction but fail on privacy, whereas FedMPDD achieves both simultaneously.

Figure 2 illustrates FedMPDD’s privacy-preserving strength under the GIA [63]. The left plot shows SSIM scores over iterations, and the right panel visualizes reconstructed CIFAR-10 samples. Laplace noise with variance 0.1 (a typical LDP setting) fails to protect data, yielding high SSIM and clear reconstructions, while variance 10 provides privacy but severely degrades model accuracy. In contrast, FedMPDD with  $m = 2000$  achieves a comparable privacy level to Laplace(10) without adding noise, since its protection arises from the  $(d - m)$ -dimensional nullspace of the projection, rigorously analyzed in Lemmas 3 and 4. At the same time, it reduces per-round communication by more than  $150\times$ , highlighting FedMPDD’s dual benefit of strong privacy and efficiency.

While increasing  $m$  accelerates convergence, it also incurs higher communication cost and potentially greater privacy leakage (as expected from Lemma 3 and 4, increasing  $m$  decreases the inherent privacy protection at a rate of  $\mathcal{O}(1/m)$ , resulting in higher SSIM scores and more successful image reconstructions). However, as illustrated, for instance, in Fig. 12 in the appendix, smaller values of  $m$  can actually achieve comparable or even faster convergence to the target accuracy, while simultaneously offering stronger privacy guarantees as a beneficial side effect. This makes FedMPDD particularly suitable for large-scale problems where both privacy and communication efficiency are critical. This behavior can be intuitively explained by the nullspace effect of the *projected directional derivative* mechanism, which effectively suppresses certain components of noise in the stochastic gradient, thereby stabilizing the optimization. For additional visualizations of another attack model [43] across different architectures, as well as full training and accuracy curves under various methods, please refer to Appendix D.

## V. CONCLUSION

We introduced FedMPDD, a novel FL framework addressing communication efficiency, which also came with some level of privacy protection, through a gradient encoding and decoding mechanism based on multi-projected directional derivatives. Building upon the single-projection FedPDD, which offered initial communication and

**TABLE IV:** Comparison of test accuracy (under a fixed communication budget), communication cost (under a target accuracy), privacy leakage, and reconstruction quality using the attack of [63] on MNIST (i.i.d.) with LeNet.

Method	Bytes Budget (GB)	Test Acc (%)	Target Acc (%)	Used Bytes (GB)	Defendability	SSIM
FedSGD	0.09	11.45	60	1.439	✗	1.00
FedSGD + Laplace (var=0.5)	0.09	11.13	60	1.611	✓	$\ll 0.03$
FedSGD + Laplace (var=1)	0.09	11.41	60	1.869	✓	$\ll 0.03$
<b>FedMPDD (m=400, 2% d)</b>	0.09	<b>77.37</b>	60	<b>0.052</b>	✓	$\ll 0.03$
<b>FedMPDD (m=600, 3% d)</b>	0.09	<b>67.75</b>	60	<b>0.079</b>	✓	$\ll 0.03$
<b>FedMPDD (m=800, 4% d)</b>	0.09	<b>58.49</b>	60	<b>0.093</b>	✓	$\ll 0.03$
QSGD (8-bit)	0.09	21.66	60	0.376	✗	0.98
Top-k (k=400)	0.09	65.75	60	0.077	✗	0.89
lp-proj	0.09	73.01	60	0.069	✗	0.75

**TABLE V:** Comparison of test accuracy (under a fixed communication budget), communication cost (under a target accuracy), privacy leakage, and reconstruction quality using the attack of [63] on CIFAR-10 (i.i.d.) with the CNN model from [1]. The symbol  $\star$  indicates that the communication budget was exceeded in the first iteration.

Method	Bytes Budget (GB)	Test Acc (%)	Target Acc (%)	Used Bytes (GB)	Defendability	SSIM
FedSGD	0.90	$\star$	60	471.96	✗	0.96
FedSGD + Laplace (var=0.1)	0.90	$\star$	60	471.96	✗	0.84
FedSGD + Laplace (var=10)	0.90	$\star$	60	not reached	✓	0.23
<b>FedMPDD (m=600, 0.2 % d)</b>	0.90	<b>40.84</b>	60	<b>1.32</b>	✓	0.14
<b>FedMPDD (m=2000, 0.6 % d)</b>	0.90	<b>36.26</b>	60	<b>3.26</b>	✓	0.22
QSGD (8-bit)	0.90	12.97	60	117.98	✗	0.93
lp-proj	0.90	34.72	60	1.84	✗	0.74
Top-k (k=600)	0.90	38.11	60	2.30	✗	0.91
SA-FedLora	0.90	35.84	60	2.10	✗	0.83

privacy benefits but suffered from dimension-dependent convergence, FedMPDD averaged multiple projections to achieve comparable convergence rates to baselines. Our theoretical analysis and empirical evaluations demonstrated FedMPDD’s superior balance of communication cost, performance, and privacy, facilitated by its efficient gradient encoding and decoding. We achieved significant uplink communication reductions compared to baseline methods, including structured, sketched, quantized, and sparsified approaches, while simultaneously ensuring robust and uniform privacy against GIAs, unlike the fluctuating and often weak privacy guarantees of LDP. The tunable parameter  $m$  allowed flexible trade-offs. Notably, smaller  $m$  values sometimes yielded faster convergence with stronger privacy. Several promising avenues remain for extending FedMPDD. First, our current privacy analysis assumes memory-bounded adversaries satisfying  $T \times m < d$ , a practically relevant model for typical federated training scenarios. Extending guarantees to unbounded-memory adversaries, as commonly modeled in cryptographic [69] and control-theoretic [65] frameworks, represents an important theoretical direction. Potential approaches include cryptographic composition with secure aggregation, information-theoretic analysis leveraging gradient evolution during training, or hybrid mechanisms combining projections with differential privacy. Second, as noted in Remark 2, client-side computational efficiency can be enhanced through the projected-forward approach, where a fixed mini-batch is sampled once and reused to compute  $m$  directional derivatives via forward-mode Jacobian-vector products (JVPs). When  $m < \frac{hpT}{h+p}$ , this approach simultaneously reduces communication overhead, enhances privacy, and lowers computational cost—crucial for resource-constrained federated devices. We plan to implement a fully optimized version leveraging efficient JVPs. Finally, since the projected directional derivative is an unbiased estimator, incorporating momentum and variance reduction techniques offers opportunities to further accelerate convergence while maintaining FedMPDD’s communication and privacy benefits.

## REFERENCES

- [1] B. McMahan, E. Moore, D. Ramage, S. Hampson, and B. A. y Arcas, “Communication-efficient learning of deep networks from decentralized data,” in *Artificial intelligence and statistics*, pp. 1273–1282, PMLR.
- [2] P. Kairouz, H. B. McMahan, B. Avent, A. Bellet, M. Bennis, A. N. Bhagoji, K. Bonawitz, Z. Charles, G. Cormode, R. Cummings, *et al.*, “Advances and open problems in federated learning,” *Foundations and trends® in machine learning*, vol. 14, no. 1–2, pp. 1–210, 2021.
- [3] J. Chen and X. Ran, “Deep learning with edge computing: A review,” *Proceedings of the IEEE*, vol. 107, no. 8, pp. 1655–1674, 2019.
- [4] T. Zeng, O. Semiaci, M. Chen, W. Saad, and M. Bennis, “Federated learning for collaborative controller design of connected and autonomous vehicles,” in *IEEE Int. Conf. on Decision and Control*, pp. 5033–5038.
- [5] H. Wang, L. F. Toso, A. Mitra, and J. Anderson, “Model-free learning with heterogeneous dynamical systems: A federated LQR approach,” *arXiv preprint arXiv:2308.11743*, 2023.
- [6] M. Chen, N. Shlezinger, H. V. Poor, Y. C. Eldar, and S. Cui, “Communication-efficient federated learning,” *Proceedings of the National Academy of Sciences*, vol. 118, no. 17, p. e2024789118, 2021.
- [7] S. Niknam, H. S. Dhillon, and J. H. Reed, “Federated learning for wireless communications: Motivation, opportunities, and challenges,” *IEEE Communications Magazine*, vol. 58, no. 6, pp. 46–51, 2020.
- [8] O. Shahid, S. Pouriyeh, R. M. Parizi, Q. Z. Sheng, G. Srivastava, and L. Zhao, “Communication efficiency in federated learning: Achievements and challenges,” *arXiv preprint arXiv:2107.10996*, 2021.
- [9] T. Li, A. K. Sahu, A. Talwalkar, and V. Smith, “Federated learning: Challenges, methods, and future directions,” *IEEE signal processing magazine*, vol. 37, no. 3, pp. 50–60, 2020.
- [10] M. Rostami, H. Moradian, and S. S. Kia, “First-order dynamic optimization for streaming convex costs,” in *2024 American Control Conference (ACC)*, pp. 2194–2199, IEEE, 2024.
- [11] P. P. Liang, T. Liu, L. Ziyin, N. B. Allen, R. P. Auerbach, D. Brent, R. Salakhutdinov, and L.-P. Morency, “Think locally, act globally: Federated learning with local and global representations,” *arXiv preprint arXiv:2001.01523*, 2020.
- [12] S. U. Stich, “Local sgd converges fast and communicates little,” *arXiv preprint arXiv:1805.09767*, 2018.
- [13] S. P. Karimireddy, S. Kale, M. Mohri, S. Reddi, S. Stich, and A. T. Suresh, “Scaffold: Stochastic controlled averaging for federated learning,” in *International conference on machine learning*, pp. 5132–5143.
- [14] F. Sattler, S. Wiedemann, K.-R. Müller, and W. Samek, “Robust and communication-efficient federated learning from non-iid data,” *IEEE transactions on neural networks and learning systems*, vol. 31, no. 9, pp. 3400–3413, 2019.
- [15] D. Alistarh, D. Grubic, J. Li, R. Tomioka, and M. Vojnovic, “Qsgd: Communication-efficient sgd via gradient quantization and encoding,” *Advances in neural information processing systems*, vol. 30, 2017.
- [16] S. Horváth, C.-Y. Ho, L. Horváth, A. N. Sahu, M. Canini, and P. Richtárik, “Natural compression for distributed deep learning,” in *Mathematical and Scientific Machine Learning*, pp. 129–141, PMLR.

[17] S. P. Karimireddy, Q. Rebjock, S. Stich, and M. Jaggi, “Error feedback fixes signsgd and other gradient compression schemes,” in *International Conference on Machine Learning*, pp. 3252–3261, PMLR.

[18] N. Shlezinger, M. Chen, Y. C. Eldar, H. V. Poor, and S. Cui, “Uveqsf: Universal vector quantization for federated learning,” *IEEE Transactions on Signal Processing*, vol. 69, pp. 500–514, 2020.

[19] J. Bernstein, Y.-X. Wang, K. Azizzadenesheli, and A. Anandkumar, “signsgd: Compressed optimisation for non-convex problems,” in *International Conference on Machine Learning*, pp. 560–569, PMLR.

[20] A. Reisizadeh, A. Mokhtari, H. Hassani, A. Jadbabaie, and R. Pedarsani, “Fedpaq: A communication-efficient federated learning method with periodic averaging and quantization,” in *International conference on artificial intelligence and statistics*, pp. 2021–2031, PMLR.

[21] A. T. Suresh, X. Y. Felix, S. Kumar, and H. B. McMahan, “Distributed mean estimation with limited communication,” in *International conference on machine learning*, pp. 3329–3337.

[22] N. Ivkin, D. Rothchild, E. Ullah, I. Stoica, R. Arora, et al., “Communication-efficient distributed SGD with sketching,” *Advances in Neural Information Processing Systems*, vol. 32, 2019.

[23] Y. Lin, S. Han, H. Mao, Y. Wang, and W. J. Dally, “Deep gradient compression: Reducing the communication bandwidth for distributed training,” *arXiv preprint arXiv:1712.01887*, 2017.

[24] E. J. Hu, Y. Shen, P. Wallis, Z. Allen-Zhu, Y. Li, S. Wang, L. Wang, W. Chen, et al., “Lora: Low-rank adaptation of large language models.,” *ICLR*, vol. 1, no. 2, p. 3, 2022.

[25] L. Yi, H. Yu, G. Wang, X. Liu, and X. Li, “Pfedlora: model-heterogeneous personalized federated learning with lora tuning,” *arXiv preprint arXiv:2310.13283*, 2023.

[26] J. Qi, Z. Luan, S. Huang, C. Fung, H. Yang, and D. Qian, “Fdllora: personalized federated learning of large language model via dual lora tuning,” *arXiv preprint arXiv:2406.07925*, 2024.

[27] T. Zhang, S. Ye, K. Zhang, J. Tang, W. Wen, M. Fardad, and Y. Wang, “A systematic dnn weight pruning framework using alternating direction method of multipliers,” in *European conference on computer vision*, pp. 184–199.

[28] K. Ullrich, E. Meeds, and M. Welling, “Soft weight-sharing for neural network compression,” *arXiv preprint arXiv:1702.04008*, 2017.

[29] D. Bertsimas, R. Cory-Wright, and J. Pauphilet, “A new perspective on low-rank optimization,” *Mathematical Programming*, vol. 202, no. 1, pp. 47–92, 2023.

[30] Y. J. Cho, L. Liu, Z. Xu, A. Fahrezi, and G. Joshi, “Heterogeneous lora for federated fine-tuning of on-device foundation models,” *arXiv preprint arXiv:2401.06432*, 2024.

[31] S. Park and W. Choi, “Regulated subspace projection based local model update compression for communication-efficient federated learning,” *IEEE Journal on Selected Areas in Communications*, vol. 41, no. 4, pp. 964–976, 2023.

[32] S. S. Azam, S. Hosseinalipour, Q. Qiu, and C. Brinton, “Recycling model updates in federated learning: Are gradient subspaces low-rank?,” in *International Conference on Learning Representations*.

[33] M. Guo, D. Liu, O. Simeone, and D. Wen, “Low-rank gradient compression with error feedback for mimo wireless federated learning,” *arXiv preprint arXiv:2401.07496*, 2024.

[34] D. Rothchild, A. Panda, E. Ullah, N. Ivkin, I. Stoica, V. Braverman, J. Gonzalez, and R. Arora, “Fetchsgd: Communication-efficient federated learning with sketching,” in *International Conference on Machine Learning*, pp. 8253–8265, PMLR.

[35] F. Haddadpour, B. Karimi, P. Li, and X. Li, “Fedsketch: Communication-efficient and private federated learning via sketching,” *arXiv preprint arXiv:2008.04975*, 2020.

[36] J. Jiang, F. Fu, T. Yang, and B. Cui, “Sketchml: Accelerating distributed machine learning with data sketches,” in *International Conference on Management of Data*, pp. 1269–1284.

[37] L. Fournier, S. Rivaud, E. Belilovsky, M. Eickenberg, and E. Oyallon, “Can forward gradient match backpropagation?,” in *International Conference on Machine Learning*, pp. 10249–10264, PMLR.

[38] M. Ren, S. Kornblith, R. Liao, and G. Hinton, “Scaling forward gradient with local losses,” *arXiv preprint arXiv:2210.03310*, 2022.

[39] D. Silver, A. Goyal, I. Danihelka, M. Hessel, and H. van Hasselt, “Learning by directional gradient descent,” in *International Conference on Learning Representations*.

[40] A. G. Baydin, B. A. Pearlmutter, D. Syme, F. Wood, and P. Torr, “Gradients without backpropagation,” *arXiv preprint arXiv:2202.08587*, 2022.

[41] M. Rostami and S. S. Kia, “Projected forward gradient-guided frank-wolfe algorithm via variance reduction,” *IEEE Control Systems Letters*, 2024.

[42] Y. Nesterov and V. Spokoiny, “Random gradient-free minimization of convex functions,” *Foundations of Computational Mathematics*, vol. 17, no. 2, pp. 527–566, 2017.

[43] L. Zhu, Z. Liu, and S. Han, “Deep leakage from gradients,” *Advances in neural information processing systems*, vol. 32, 2019.

[44] B. Zhao, K. R. Mopuri, and H. Bilen, “Idlg: Improved deep leakage from gradients,” *arXiv preprint arXiv:2001.02610*, 2020.

[45] Y. Huang, S. Gupta, Z. Song, K. Li, and S. Arora, “Evaluating gradient inversion attacks and defenses in federated learning,” *Advances in neural information processing systems*, vol. 34, pp. 7232–7241, 2021.

[46] H. Yin, A. Mallya, A. Vahdat, J. M. Alvarez, J. Kautz, and P. Molchanov, “See through gradients: Image batch recovery via gradinversion,” in *Proceedings of the IEEE/CVF conference on computer vision and pattern recognition*, pp. 16337–16346.

[47] L. Melis, C. Song, E. De Cristofaro, and V. Shmatikov, “Exploiting unintended feature leakage in collaborative learning,” in *IEEE symposium on security and privacy*, pp. 691–706.

[48] Z. Li, L. Wang, G. Chen, Z. Zhang, M. Shafiq, and Z. Gu, “E2egi: End-to-end gradient inversion in federated learning,” *IEEE Journal of Biomedical and Health Informatics*, vol. 27, no. 2, pp. 756–767, 2022.

[49] K. Wei, J. Li, M. Ding, C. Ma, H. H. Yang, F. Farokhi, S. Jin, T. Q. Quek, and H. V. Poor, “Federated learning with differential privacy: Algorithms and performance analysis,” *IEEE transactions on information forensics and security*, vol. 15, pp. 3454–3469, 2020.

[50] S. Truex, L. Liu, K.-H. Chow, M. E. Gursoy, and W. Wei, “Ldp-fed: Federated learning with local differential privacy,” in *Proceedings of the third ACM international workshop on edge systems, analytics and networking*, pp. 61–66.

[51] Y. Zhao, J. Zhao, M. Yang, T. Wang, N. Wang, L. Lyu, D. Niyato, and K.-Y. Lam, “Local differential privacy-based federated learning for internet of things,” *IEEE Internet of Things Journal*, vol. 8, no. 11, pp. 8836–8853, 2020.

[52] M. Seif, R. Tandon, and M. Li, “Wireless federated learning with local differential privacy,” in *IEEE International Symposium on Information Theory*, pp. 2604–2609.

[53] M. S. Jere, T. Farnan, and F. Koushanfar, “A taxonomy of attacks on federated learning,” *IEEE Security & Privacy*, vol. 19, no. 2, pp. 20–28, 2020.

[54] S. Amiri, A. Belloum, S. Klous, and L. Gommans, “Compressive differentially private federated learning through universal vector quantization,” in *AAAI Workshop on Privacy-Preserving Artificial Intelligence*, pp. 2–9.

[55] L. Lyu, “Dp-signsgd: When efficiency meets privacy and robustness,” *arXiv preprint arXiv:2105.04808*, 2021.

[56] N. Lang, E. Sofer, T. Shaked, and N. Shlezinger, “Joint privacy enhancement and quantization in federated learning,” *IEEE Transactions on Signal Processing*, vol. 71, pp. 295–310, 2023.

[57] N. Agarwal, A. T. Suresh, F. X. X. Yu, S. Kumar, and H. B. McMahan, “Cpsgd: Communication-efficient and differentially-private distributed sgd,” *Advances in Neural Information Processing Systems*, vol. 31, 2018.

[58] R. A. Horn and C. R. Johnson, *Matrix analysis*. Cambridge university press, 2012.

[59] C. T. Dinh, N. Tran, and J. Nguyen, “Personalized federated learning with moreau envelopes,” *Advances in neural information processing systems*, vol. 33, pp. 21394–21405, 2020.

[60] K. Liu, S. Hu, S. Z. Wu, and V. Smith, “On privacy and personalization in cross-silo federated learning,” *Advances in neural information processing systems*, vol. 35, pp. 5925–5940, 2022.

[61] M. Rostami and S. S. Kia, “Federated learning using variance reduced stochastic gradient for probabilistically activated agents,” in *2023 American Control Conference (ACC)*, pp. 861–866, IEEE.

[62] R. Vershynin, *High-dimensional probability: An introduction with applications in data science*, vol. 47. Cambridge university press, 2018.

[63] W. Yu, H. Fang, B. Chen, X. Sui, C. Chen, H. Wu, S.-T. Xia, and K. Xu, “Gi-nas: Boosting gradient inversion attacks through adaptive neural architecture search,” *IEEE Transactions on Information Forensics and Security*, 2025.

[64] J. Geiping, H. Bauermeister, H. Dröge, and M. Moeller, “Inverting gradients—how easy is it to break privacy in federated learning?,” *Advances in neural information processing systems*, vol. 33, pp. 16937–16947, 2020.

[65] A. Teixeira, I. Shames, H. Sandberg, and K. H. Johansson, “A secure control framework for resource-limited adversaries,” *Automatica*, vol. 51, pp. 135–148, 2015.

[66] S. Lin, Y. Han, X. Li, and Z. Zhang, “Personalized federated learning towards communication efficiency, robustness and fairness,” *Advances in Neural Information Processing Systems*, vol. 35, pp. 30471–30485, 2022.

- [67] Y. Yang, H. Yu, C. Sun, T. Gao, X. Liu, X. Xu, P. Zhang, and G. Wang, “Spd-clf: Stepwise parameter dropout for efficient continual federated learning,” *arXiv preprint arXiv:2405.09394*, 2024.
- [68] D. Alistarh, T. Hoefler, M. Johansson, N. Konstantinov, S. Khirirat, and C. Renggli, “The convergence of sparsified gradient methods,” *Advances in Neural Information Processing Systems*, vol. 31, 2018.
- [69] C. Dwork, F. McSherry, K. Nissim, and A. Smith, “Calibrating noise to sensitivity in private data analysis,” in *Theory of Cryptography Conference*.

## APPENDIX

### A. Gradient Inversion Attacks and Deep Leakage from Gradients

Gradient inversion attacks (GIAs) are privacy threats in federated learning where an adversary attempts to reconstruct a client’s private training data from transmitted gradients [43]–[46], [64]. Since gradients encode information about the input data through the loss function’s derivatives, an adversary observing full-dimensional gradients  $\mathbf{g}_i(\mathbf{x}_k) \in \mathbb{R}^d$  can potentially invert them to recover sensitive information such as images or text. GIAs may operate on a single gradient observation (snapshot) or leverage multiple rounds of observations. These attacks reveal a critical vulnerability in standard FL protocols and motivate the development of privacy-preserving methods.

As a concrete example employed in our empirical evaluations, we describe Deep Leakage from Gradients (DLG) [43], an optimization-based attack that reconstructs private training data from a single observed gradient. Given only the observed gradient  $\mathbf{g}_i(\mathbf{x})$  computed on an *unknown* data pair  $(\mathbf{v}, y)$ , the attacker reconstructs  $(\mathbf{v}, y)$  through the following iterative procedure:

leftrmargin=1.6em

- 1) *Initialization.* The attacker initializes dummy inputs and labels  $\mathbf{v}'_1 \sim \mathcal{N}(0, 1)$  and  $y'_1 \sim \mathcal{N}(0, 1)$ .
- 2) *Dummy Gradient Computation.* At iteration  $i$ , the attacker computes the dummy gradient

$$\mathbf{g}'_i(\mathbf{x}) = \frac{\partial f(F(\mathbf{v}'_i; \mathbf{x}), y'_i)}{\partial \mathbf{x}},$$

where  $F$  is the model architecture and  $f$  is the loss function (e.g., cross-entropy).

- 3) *Matching Objective.* The discrepancy

$$D_i = \|\mathbf{g}'_i(\mathbf{x}) - \mathbf{g}_i(\mathbf{x})\|_2^2$$

measures how closely the dummy data reproduce the observed gradient.

- 4) *Dummy Data Update.* Using gradient-based optimization (commonly Adam or L-BFGS), the attacker updates:

$$\mathbf{v}'_{i+1} = \mathbf{v}'_i - \alpha \nabla_{\mathbf{v}'} D_i, \quad y'_{i+1} = y'_i - \alpha \nabla_{y'} D_i,$$

where  $\alpha$  is the learning rate.

After several hundred to a few thousand iterations, the optimized pair  $(\mathbf{v}', y')$  can closely approximate the original input. The reconstruction quality depends critically on the information content of the observed gradient: full-dimensional gradients enable highly accurate reconstruction, while obfuscated or compressed gradients reduce the attacker’s ability to recover private data.

DLG and similar GIAs reveal fundamental privacy vulnerabilities in standard FL protocols. This motivates privacy-preserving methods such as differential privacy (adding noise to gradients), secure aggregation (cryptographic masking), or our proposed FedMPDD, which inherently obfuscates gradients through rank-deficient projections that create ambiguity without requiring explicit noise addition or cryptographic overhead.

### B. Details and Proofs

Below we present omitted proofs and lemmas for the auxiliary and main results presented in the paper.

*Proof:* [Proof of Lemma 1] Recall the variance formula

$$\text{Var}[\hat{\mathbf{g}}(\mathbf{x})] = \mathbb{E}[\hat{\mathbf{g}}(\mathbf{x}) \hat{\mathbf{g}}(\mathbf{x})^\top] - \mathbb{E}[\hat{\mathbf{g}}(\mathbf{x})]\mathbb{E}[\hat{\mathbf{g}}(\mathbf{x})]^\top. \quad (\text{B.1})$$

We compute  $\text{Var}[\hat{\mathbf{g}}(\mathbf{x})]$  for the cases where  $\mathbf{u}$  is drawn from either a normal or rademacher distribution. First, we begin with the case where  $\mathbf{u} \sim \mathcal{N}(\mathbf{0}, \mathbf{I}_d)$ . Recall, for a random vector  $\mathbf{u} \sim \mathcal{N}(\mathbf{0}, \mathbf{I}_d)$ ,

$$\mathbb{E}[\mathbf{u}] = \mathbf{0}, \quad \mathbb{E}[\mathbf{u}\mathbf{u}^\top] = \mathbf{I}_d.$$

Thus, we have  $\mathbb{E}[\hat{\mathbf{g}}(\mathbf{x})] = \mathbf{g}(\mathbf{x})$ . Next, compute  $\mathbb{E}[\hat{\mathbf{g}}(\mathbf{x})\hat{\mathbf{g}}(\mathbf{x})^\top]$  in (B.1)

$$\mathbb{E}[\hat{\mathbf{g}}(\mathbf{x})\hat{\mathbf{g}}(\mathbf{x})^\top] = \mathbb{E}[(\mathbf{u}^\top \mathbf{g}(\mathbf{x}))^2 \mathbf{u}\mathbf{u}^\top]. \quad (\text{B.2})$$

Note that,  $\mathbf{u}\mathbf{u}^\top = \sum_{m=1}^d \sum_{p=1}^d u_m u_p \mathbf{e}_m \mathbf{e}_p^\top$  and  $(\mathbf{u}^\top \mathbf{g}(\mathbf{x}))^2 = (\sum_{l=1}^d u_l g_l(\mathbf{x}))^2 = \sum_{l=1}^d \sum_{n=1}^d u_l u_n g_l(\mathbf{x}) g_n(\mathbf{x})$ , where  $\mathbf{e}$  is the basis vector.

Plugging back into (B.2), we have

$$\begin{aligned} & \mathbb{E}[\hat{\mathbf{g}}(\mathbf{x})\hat{\mathbf{g}}(\mathbf{x})^\top] \\ &= \mathbb{E}[\sum_{l=1}^d \sum_{n=1}^d u_l u_n g_l(\mathbf{x}) g_n(\mathbf{x}) \sum_{m=1}^d \sum_{p=1}^d u_m u_p \mathbf{e}_m \mathbf{e}_p^\top] \\ &= \mathbb{E}[\sum_{l=1}^d \sum_{n=1}^d \sum_{m=1}^d \sum_{p=1}^d u_l u_n g_l(\mathbf{x}) g_n(\mathbf{x}) u_m u_p \mathbf{e}_m \mathbf{e}_p^\top] \\ &= \sum_{l=1}^d \sum_{n=1}^d \sum_{m=1}^d \sum_{p=1}^d g_l(\mathbf{x}) g_n(\mathbf{x}) \mathbb{E}[u_l u_n u_m u_p] \mathbf{e}_m \mathbf{e}_p^\top. \end{aligned} \quad (\text{B.3})$$

Note that, the last equality comes from the fact that  $\mathbf{u}$  is independent from  $\mathbf{g}(\mathbf{x})$ . Now, there are different cases that  $\mathbb{E}[u_l u_n u_m u_p]$  is non-zero in (B.3).

Case 1 ( $l = n$  and  $m = p$ ): In this case, (B.3) simplifies to the following

$$\mathbb{E}[\hat{\mathbf{g}}(\mathbf{x})\hat{\mathbf{g}}(\mathbf{x})^\top] = \sum_{l=1}^d \sum_{m=1}^d g_l^2(\mathbf{x}) \mathbb{E}[u_l^2] \mathbb{E}[u_m^2] \mathbf{e}_m \mathbf{e}_m^\top = \|\mathbf{g}(\mathbf{x})\|^2 \mathbf{I}_d.$$

Case 2 ( $l = m$  and  $n = p$ ): In this case, (B.3) simplifies to the following

$$\begin{aligned} \mathbb{E}[\hat{\mathbf{g}}(\mathbf{x})\hat{\mathbf{g}}(\mathbf{x})^\top] &= \sum_{l=1}^d \sum_{n=1}^d g_l(\mathbf{x}) g_n(\mathbf{x}) \mathbb{E}[u_l^2] \mathbb{E}[u_n^2] \mathbf{e}_l \mathbf{e}_n^\top \\ &= \mathbf{g}(\mathbf{x}) (\mathbf{g}(\mathbf{x}))^\top \end{aligned}$$

Case 3 ( $l = p$  and  $m = n$ ): Similar to case 2, (B.3) simplifies to the following

$$\mathbb{E}[\hat{\mathbf{g}}(\mathbf{x})\hat{\mathbf{g}}(\mathbf{x})^\top] = \mathbf{g}(\mathbf{x}) (\mathbf{g}(\mathbf{x}))^\top$$

Case 4 ( $l = n = m = p$ ): In this case, (B.3) simplifies to the following

$$\mathbb{E}[\hat{\mathbf{g}}(\mathbf{x})\hat{\mathbf{g}}(\mathbf{x})^\top] = \sum_{l=1}^d g_l^2(\mathbf{x}) \mathbb{E}[u_l^4] \mathbf{e}_l \mathbf{e}_l^\top = 3 \|\mathbf{g}(\mathbf{x})\|^2 \mathbf{I}_d$$

Then, (B.3) can be simplified as follows

$$\mathbb{E}[\hat{\mathbf{g}}(\mathbf{x})\hat{\mathbf{g}}(\mathbf{x})^\top] = 2 \mathbf{g}(\mathbf{x}) (\mathbf{g}(\mathbf{x}))^\top + 4 \|\mathbf{g}(\mathbf{x})\|^2 \mathbf{I}_d.$$

As a result, (B.1) can be written as follows for the case where  $\mathbf{u}$  is drawn from a normal distribution with zero mean and unit variance.

$$\text{Var}_{\mathbf{u} \sim \mathcal{N}(\mathbf{0}, \mathbf{I}_d)}[\hat{\mathbf{g}}(\mathbf{x})] = \mathbf{g}(\mathbf{x}) (\mathbf{g}(\mathbf{x}))^\top + 4 \|\mathbf{g}(\mathbf{x})\|^2 \mathbf{I}_d. \quad (\text{B.4})$$

Now, we compute the variance  $\text{Var}[\hat{\mathbf{g}}(\mathbf{x})]$  in the case where  $\mathbf{u} \sim \text{Rademacher}^d$ . Recall that for a random vector  $\mathbf{u}$  with i.i.d. Rademacher entries, we have  $\mathbb{E}[\mathbf{u}] = \mathbf{0}$  and  $\mathbb{E}[\mathbf{u}\mathbf{u}^\top] = \mathbf{I}_d$ .

Therefore, we have  $\mathbb{E}[\hat{\mathbf{g}}(\mathbf{x})] = \mathbf{g}(\mathbf{x})$ .

Similar to the proof for the normal distribution, cases 1, 2, and 3 are identical. However in the fourth case, where  $l = n = m = p$ , since the fourth moment of a Rademacher distribution is 1, we get  $\mathbb{E}[\hat{\mathbf{g}}(\mathbf{x})\hat{\mathbf{g}}(\mathbf{x})^\top] = \|\mathbf{g}(\mathbf{x})\|^2 \mathbf{I}_d$ . Then, (B.3) can be simplified as follows

$$\mathbb{E}[\hat{\mathbf{g}}(\mathbf{x})\hat{\mathbf{g}}(\mathbf{x})^\top] = 2\mathbf{g}(\mathbf{x})(\mathbf{g}(\mathbf{x}))^\top + 2\|\mathbf{g}(\mathbf{x})\|^2 \mathbf{I}_d.$$

Thus, we get

$$\text{Var}_{\mathbf{u} \sim \text{Rademacher}^d}[\hat{\mathbf{g}}(\mathbf{x})] = \mathbf{g}(\mathbf{x})(\mathbf{g}(\mathbf{x}))^\top + 2\|\mathbf{g}(\mathbf{x})\|^2 \mathbf{I}_d. \quad (\text{B.5})$$

From (B.4) and (B.5), we have the following

$$\text{Var}_{\mathbf{u} \sim \mathcal{N}(\mathbf{0}, \mathbf{I}_d)}[\hat{\mathbf{g}}(\mathbf{x})] - \text{Var}_{\mathbf{u} \sim \text{Rademacher}^d}[\hat{\mathbf{g}}(\mathbf{x})] = 2\|\mathbf{g}(\mathbf{x})\|^2 \mathbf{I}_d \quad (\text{B.6})$$

which concludes the proof.  $\blacksquare$

*Proof:* [Proof of Lemma 3] Note that for a single direction  $\mathbf{u}_{k,i}$  ( $m = 1$ ),

$$\begin{aligned} \|\hat{\mathbf{g}}_i(\mathbf{x}_k)\|^2 &= \mathbf{u}_{k,i}^\top (\mathbf{u}_{k,i}^\top \mathbf{g}_i(\mathbf{x}_k)) (\mathbf{u}_{k,i}^\top \mathbf{g}_i(\mathbf{x}_k)) \mathbf{u}_{k,i} \\ &= (\mathbf{u}_{k,i}^\top \mathbf{u}_{k,i}) (\mathbf{g}_i(\mathbf{x}_k)^\top \mathbf{u}_{k,i} \mathbf{u}_{k,i}^\top \mathbf{g}_i(\mathbf{x}_k)). \end{aligned} \quad (\text{B.7})$$

Since for Rademacher  $\mathbf{u}_{k,i}$ , we have  $\mathbf{u}_{k,i}^\top \mathbf{u}_{k,i} = d$ , it follows that

$$\mathbb{E}_{\mathbf{u}}[\|\hat{\mathbf{g}}_i(\mathbf{x}_k)\|^2] = d \mathbf{g}_i(\mathbf{x}_k)^\top \mathbb{E}_{\mathbf{u}}[\mathbf{u}_{k,i} \mathbf{u}_{k,i}^\top] \mathbf{g}_i(\mathbf{x}_k) = d \|\mathbf{g}_i(\mathbf{x}_k)\|^2.$$

Therefore, since the estimator satisfies

$$\mathbb{E}_{\mathbf{u}}[\hat{\mathbf{g}}_i(\mathbf{x}_k)] = \mathbf{g}_i(\mathbf{x}_k),$$

we obtain for one direction

$$\begin{aligned} \mathbb{E}_{\mathbf{u}}[\|\hat{\mathbf{g}}_i(\mathbf{x}_k) - \mathbf{g}_i(\mathbf{x}_k)\|^2] &= \mathbb{E}_{\mathbf{u}}[\|\hat{\mathbf{g}}_i(\mathbf{x}_k)\|^2 - \|\mathbf{g}_i(\mathbf{x}_k)\|^2] \\ &= (d-1) \|\mathbf{g}_i(\mathbf{x}_k)\|^2. \end{aligned} \quad (\text{B.8})$$

Now extend to  $m$  directions. The multi-direction estimator is

$$\hat{\mathbf{g}}_i(\mathbf{x}_k) = \frac{1}{m} \sum_{j=1}^m \mathbf{u}_{k,i}^{(j)} (\mathbf{u}_{k,i}^{(j)})^\top \mathbf{g}_i(\mathbf{x}_k).$$

Because the  $\mathbf{u}_{k,i}^{(j)}$  are independent and identically distributed, the cross terms vanish in expectation, and all diagonal terms are the same. Thus,

$$\mathbb{E}[\|\hat{\mathbf{g}}_i(\mathbf{x}_k) - \mathbf{g}_i(\mathbf{x}_k)\|^2] = \frac{1}{m} (d-1) \|\mathbf{g}_i(\mathbf{x}_k)\|^2.$$

Dividing both sides by  $\|\mathbf{g}_i(\mathbf{x}_k)\|^2$  yields in (9).  $\blacksquare$

*Proof:* [Proof of Lemma 4] Consider the reconstruction loss

$$\begin{aligned} \mathcal{L}(\hat{v}) &= \left\| \frac{1}{m} \mathbf{U}_{k,i} \mathbf{U}_{k,i}^\top \mathbf{g}_i(v, c; \mathbf{x}_k) - \mathbf{g}_i(\hat{v}, c; \mathbf{x}_k) \right\| \\ &= \left\| (\mathbf{g}_i(v, c; \mathbf{x}_k) - \mathbf{g}_i(\hat{v}, c; \mathbf{x}_k)) - \right. \\ &\quad \left. (\mathbf{g}_i(v, c; \mathbf{x}_k) - \frac{1}{m} \mathbf{U}_{k,i} \mathbf{U}_{k,i}^\top \mathbf{g}_i(v, c; \mathbf{x}_k)) \right\| \\ &\geq \left| \|\mathbf{g}_i(v, c; \mathbf{x}_k) - \frac{1}{m} \mathbf{U}_{k,i} \mathbf{U}_{k,i}^\top \mathbf{g}_i(v, c; \mathbf{x}_k)\| - \right. \\ &\quad \left. \|\mathbf{g}_i(v, c; \mathbf{x}_k) - \mathbf{g}_i(\hat{v}, c; \mathbf{x}_k)\| \right| \\ &\geq \|(I - \frac{1}{m} \mathbf{U}_{k,i} \mathbf{U}_{k,i}^\top) \mathbf{g}_i(v, c; \mathbf{x}_k)\| - \\ &\quad \|\mathbf{g}_i(v, c; \mathbf{x}_k) - \mathbf{g}_i(\hat{v}, c; \mathbf{x}_k)\|. \end{aligned}$$

Thus,  $\|\mathbf{g}_i(v, c; \mathbf{x}_k) - \mathbf{g}_i(\hat{v}, c; \mathbf{x}_k)\| \geq \text{proj}_g(v, c; \mathbf{x}_k, \mathbf{U}_{k,i}) - \mathcal{L}(\hat{v})$ , where  $\text{proj}_g(v, c; \mathbf{x}_k, \mathbf{U}_{k,i}) := \|(I - \frac{1}{m} \mathbf{U}_{k,i} \mathbf{U}_{k,i}^\top) \mathbf{g}_i(v, c; \mathbf{x}_k)\|$  denotes the projection-induced gradient error.

Assuming that for fixed  $\mathbf{x}_k$  and known  $c$ , the map  $v \mapsto \mathbf{g}_i(v, c; \mathbf{x}_k)$

is  $L_v(\mathbf{x}_k)$ -Lipschitz (as is satisfied by standard models), we obtain

$$\|v - \hat{v}\| \geq \frac{\text{proj}_g(v, c; \mathbf{x}_k, \mathbf{U}_{k,i}) - \mathcal{L}(\hat{v})}{L_v(\mathbf{x}_k)}.$$

With the convention that the right-hand side is interpreted as  $\max\{0, \cdot\}$ , in particular for an attack-optimal recovery  $\hat{v}^* \in \arg \min_{\hat{v}} \mathcal{L}(\hat{v})$ ,

$$\begin{aligned} \|v - \hat{v}^*\| &\geq \frac{\text{proj}_g(v, c; \mathbf{x}_k, \mathbf{U}_{k,i}) - \mathcal{L}(\hat{v}^*)}{L_v(\mathbf{x}_k)}, \\ \text{and if } \mathcal{L}(\hat{v}^*) = 0, \quad \|v - \hat{v}^*\| &\geq \frac{\text{proj}_g(v, c; \mathbf{x}_k, \mathbf{U}_{k,i})}{L_v(\mathbf{x}_k)}. \end{aligned} \quad (\text{B.9})$$

Squaring the above bound, taking expectation with respect to  $\mathbf{U}_{k,i}$ , and invoking Lemma 3, we arrive at

$$\begin{aligned} \mathbb{E}[\|v - \hat{v}^*\|^2] &\geq \frac{1}{L_v(\mathbf{x}_k)^2} \mathbb{E}[\text{proj}_g(v, c; \mathbf{x}_k, \mathbf{U}_{k,i})^2] \\ &= \frac{d-1}{m L_v(\mathbf{x}_k)^2} \|\mathbf{g}_i(v, c; \mathbf{x}_k)\|^2. \end{aligned} \quad (\text{B.10})$$

Here, we used the fact that from Lemma 3, i.e.,

$$\mathbb{E}[\text{proj}_g(v, c; \mathbf{x}_k, \mathbf{U}_{k,i})^2] = \frac{d-1}{m} \|\mathbf{g}_i(v, c; \mathbf{x}_k)\|^2. \quad \blacksquare$$

*Proof:* [Proof of Theorem 1] Since  $f$  is  $L$ -smooth, we can write

$$\begin{aligned} \mathbb{E}[f(\mathbf{x}_{k+1})|\mathbf{x}_k] &\leq f(\mathbf{x}_k) + \langle \nabla f(\mathbf{x}_k), \mathbb{E}[\mathbf{x}_{k+1} - \mathbf{x}_k|\mathbf{x}_k] \rangle \\ &\quad + \frac{L}{2} \mathbb{E}[\|\mathbf{x}_{k+1} - \mathbf{x}_k\|^2|\mathbf{x}_k], \end{aligned} \quad (\text{B.11})$$

from line 14 of FedPDD algorithm into (B.11), we have

$$\begin{aligned} \mathbb{E}[f(\mathbf{x}_{k+1})|\mathbf{x}_k] &\leq f(\mathbf{x}_k) - \eta \langle \nabla f(\mathbf{x}_k), \mathbb{E}[\hat{\mathbf{g}}(\mathbf{x}_k)|\mathbf{x}_k] \rangle \\ &\quad + \frac{L\eta^2}{2} \mathbb{E}[\|\hat{\mathbf{g}}(\mathbf{x}_k)\|^2|\mathbf{x}_k], \\ &= f(\mathbf{x}_k) - \eta \|\nabla f(\mathbf{x}_k)\|^2 + \frac{L\eta^2}{2} \mathbb{E}[\|\hat{\mathbf{g}}(\mathbf{x}_k) - \nabla f(\mathbf{x}_k)\|^2|\mathbf{x}_k] \\ &\quad + \|\nabla f(\mathbf{x}_k)\|^2, \\ &= f(\mathbf{x}_k) - \left(\eta - \frac{L\eta^2}{2}\right) \|\nabla f(\mathbf{x}_k)\|^2 \\ &\quad + \frac{L\eta^2}{2} \mathbb{E}[\|\hat{\mathbf{g}}(\mathbf{x}_k) - \nabla f(\mathbf{x}_k)\|^2|\mathbf{x}_k], \end{aligned} \quad (\text{B.12})$$

where the first equality comes from the unbiasedness of  $\hat{\mathbf{g}}(\mathbf{x}_k)$ , i.e.,  $\mathbb{E}[\hat{\mathbf{g}}(\mathbf{x}_k)|\mathbf{x}_k] = \nabla f(\mathbf{x}_k)$ , the second equality comes from bias-variance decomposition of  $\mathbb{E}[\|\hat{\mathbf{g}}(\mathbf{x}_k)\|^2|\mathbf{x}_k]$ . Provided that  $\eta < \frac{1}{L}$ , and taking total expectation on both sides of (B.12) we have

$$\begin{aligned} \mathbb{E}[f(\mathbf{x}_{k+1})] &\leq \mathbb{E}[f(\mathbf{x}_k)] - \frac{\eta}{2} \mathbb{E}[\|\nabla f(\mathbf{x}_k)\|^2] \\ &\quad + \frac{L\eta^2}{2} \mathbb{E}[\|\hat{\mathbf{g}}(\mathbf{x}_k) - \nabla f(\mathbf{x}_k)\|^2], \end{aligned} \quad (\text{B.13})$$

First we simplify the second summand in the upper bound of (B.13)

by adding and subtracting  $\frac{1}{\beta N} \sum_{i \in \mathcal{A}_k} \mathbf{g}_i(\mathbf{x}_k)$ , which leads to

$$\begin{aligned}
\mathbb{E}[\|\hat{\mathbf{g}}(\mathbf{x}_k) - \nabla f(\mathbf{x}_k)\|^2] &= \mathbb{E}[\|\frac{1}{\beta N} \sum_{i \in \mathcal{A}_k} \mathbf{g}_i(\mathbf{x}_k) - \nabla f(\mathbf{x}_k) \\
&\quad + \hat{\mathbf{g}}(\mathbf{x}_k) - \frac{1}{\beta N} \sum_{i \in \mathcal{A}_k} \mathbf{g}_i(\mathbf{x}_k)\|^2] \\
&\leq 2\mathbb{E}[\|\frac{1}{\beta N} \sum_{i \in \mathcal{A}_k} \mathbf{g}_i(\mathbf{x}_k) - \nabla f(\mathbf{x}_k)\|^2] + 2\mathbb{E}[\|\hat{\mathbf{g}}(\mathbf{x}_k) \\
&\quad - \frac{1}{\beta N} \sum_{i \in \mathcal{A}_k} \mathbf{g}_i(\mathbf{x}_k)\|^2] \\
&= 2\mathbb{E}[\|\frac{1}{\beta N} \sum_{i \in \mathcal{A}_k} \mathbf{g}_i(\mathbf{x}_k) - \nabla f(\mathbf{x}_k)\|^2] \\
&\quad + 2\mathbb{E}[\|\frac{1}{\beta N} \sum_{i \in \mathcal{A}_k} s_i^k \mathbf{u}_{k,i} - \frac{1}{\beta N} \sum_{i \in \mathcal{A}_k} \mathbf{g}_i(\mathbf{x}_k)\|^2] \\
&\leq 2\mathbb{E}[\|\frac{1}{\beta N} \sum_{i \in \mathcal{A}_k} \mathbf{g}_i(\mathbf{x}_k) - \nabla f(\mathbf{x}_k)\|^2] \\
&\quad + \frac{2}{\beta N} \sum_{i \in \mathcal{A}_k} \mathbb{E}[\|s_i^k \mathbf{u}_{k,i} - \mathbf{g}_i(\mathbf{x}_k)\|^2], \tag{B.14}
\end{aligned}$$

where the first inequality follows from  $\|a + b\|^2 \leq 2\|a\|^2 + 2\|b\|^2$ , and the second inequality follows from Jensen's inequality.

Next, we note that using [59, Lemma 4] we can write

$$\begin{aligned}
\mathbb{E}_{\mathcal{A}_k} \left\| \frac{1}{\beta N} \sum_{i \in \mathcal{A}_k} \nabla f_i(\mathbf{x}_k) - \nabla f(\mathbf{x}_k) \right\|_2^2 &\leq \\
\frac{1/\beta - 1}{N-1} \cdot \frac{1}{N} \sum_{i=1}^N \|\nabla f_i(\mathbf{x}_k) - \nabla f(\mathbf{x}_k)\|_2^2, \tag{B.15}
\end{aligned}$$

which along with (B.14) leads to

$$\begin{aligned}
\mathbb{E}[\|\hat{\mathbf{g}}(\mathbf{x}_k) - \nabla f(\mathbf{x}_k)\|^2] &\leq \frac{2(1/\beta - 1)}{N(N-1)} \sum_{i=1}^N \mathbb{E}[\|\nabla f_i(\mathbf{x}_k) - \\
&\quad \nabla f(\mathbf{x}_k)\|^2] + \frac{2}{\beta N} \sum_{i \in \mathcal{A}_k} \mathbb{E}[\|s_i^k \mathbf{u}_{k,i} - \mathbf{g}_i(\mathbf{x}_k)\|^2], \\
&= \frac{2(1/\beta - 1)}{N(N-1)} \sum_{i=1}^N \mathbb{E}[\|\nabla f_i(\mathbf{x}_k) - \nabla f(\mathbf{x}_k)\|^2] \\
&\quad + \frac{2}{\beta N} \sum_{i \in \mathcal{A}_k} \mathbb{E}[\|\hat{\mathbf{g}}_i(\mathbf{x}_k) - \mathbf{g}_i(\mathbf{x}_k)\|^2], \tag{B.16}
\end{aligned}$$

where the equality comes from the fact that  $s_i^k \mathbf{u}_{k,i} = \hat{\mathbf{g}}_i(\mathbf{x}_k)$ . Now, using the result from Lemma 3, (B.16) leads to

$$\begin{aligned}
\mathbb{E}[\|\hat{\mathbf{g}}(\mathbf{x}_k) - \nabla f(\mathbf{x}_k)\|^2] &\leq \frac{2(1/\beta - 1)}{N(N-1)} \sum_{i=1}^N \mathbb{E}[\|\nabla f_i(\mathbf{x}_k) - \\
&\quad \nabla f(\mathbf{x}_k)\|^2] + \frac{2(d-1)}{\beta N} \sum_{i \in \mathcal{A}_k} \mathbb{E}[\|\mathbf{g}_i(\mathbf{x}_k)\|^2]. \tag{B.17}
\end{aligned}$$

Subsequently, given (B.17), we obtain from (B.13):

$$\begin{aligned}
\mathbb{E}[f(\mathbf{x}_{k+1})] &\leq \mathbb{E}[f(\mathbf{x}_k)] - \frac{\eta}{2} \mathbb{E}[\|\nabla f(\mathbf{x}_k)\|^2] \\
&\quad + \frac{L\eta^2}{2} \left( \frac{2(1/\beta - 1)}{N(N-1)} \sum_{i=1}^N \mathbb{E}[\|\nabla f_i(\mathbf{x}_k) - \nabla f(\mathbf{x}_k)\|^2] \right. \\
&\quad \left. + \frac{2(d-1)}{\beta N} \sum_{i \in \mathcal{A}_k} \mathbb{E}[\|\mathbf{g}_i(\mathbf{x}_k)\|^2] \right). \tag{B.18}
\end{aligned}$$

Invoking Assumption 1, which bounds the variance of local gradients relative to the global gradient in (B.18), we get

$$\begin{aligned}
\mathbb{E}[f(\mathbf{x}_{k+1})] &\leq \mathbb{E}[f(\mathbf{x}_k)] - \frac{\eta}{2} \mathbb{E}[\|\nabla f(\mathbf{x}_k)\|^2] + \\
&\quad \frac{L\eta^2}{2} \left( \frac{2(1/\beta - 1)}{N-1} \sigma^2 + \frac{2(d-1)}{\beta N} \sum_{i \in \mathcal{A}_k} \mathbb{E}[\|\mathbf{g}_i(\mathbf{x}_k)\|^2] \right). \tag{B.19}
\end{aligned}$$

Rearranging and summing  $k$  from 0 to  $K-1$  in (B.19), we have

$$\begin{aligned}
\frac{1}{K} \sum_{k=0}^{K-1} \mathbb{E}[\|\nabla f(\mathbf{x}_k)\|^2] &\leq \frac{2}{K\eta} (\mathbb{E}[f(\mathbf{x}_0)] - \mathbb{E}[f(\mathbf{x}_K)]) + \\
\frac{2L\eta(1/\beta - 1)}{K(N-1)} \sigma^2 &+ \frac{2L\eta(d-1)}{K\beta N} \sum_{k=0}^{K-1} \sum_{i \in \mathcal{A}_k} \mathbb{E}[\|\mathbf{g}_i(\mathbf{x}_k)\|^2] \\
&\leq \frac{2}{K\eta} (\mathbb{E}[f(\mathbf{x}_0)] - f^*) + \frac{2L\eta(1/\beta - 1)}{K(N-1)} \sigma^2 \\
&+ \frac{2L\eta(d-1)}{K\beta N} \sum_{k=0}^{K-1} \sum_{i \in \mathcal{A}_k} \mathbb{E}[\|\mathbf{g}_i(\mathbf{x}_k)\|^2]. \tag{B.20}
\end{aligned}$$

We simplify the upper bound in (B.20) by invoking Assumption 1 on the bounded variance of the stochastic gradient, we get

$$\begin{aligned}
\frac{1}{K} \sum_{k=0}^{K-1} \mathbb{E}[\|\nabla f(\mathbf{x}_k)\|^2] &\leq \frac{2}{K\eta} (f(\mathbf{x}_0) - f^*) \\
&+ \frac{2L\eta(1/\beta - 1)}{K(N-1)} \sigma^2 + 2L\eta d G^2. \tag{B.21}
\end{aligned}$$

If we set  $\eta = \frac{1}{L\sqrt{K}}$  in (B.21), we have a convergence rate of  $\mathcal{O}(d/\sqrt{K})$  to a stationary point of  $f(\mathbf{x})$ .  $\blacksquare$

*Proof:* [Proof of Theorem 2] For notational convenience, we stack the  $m$  random direction vectors into a single matrix  $\mathbf{U}_{k,i} = [\mathbf{u}_{k,i}^{(1)} \mathbf{u}_{k,i}^{(2)} \dots \mathbf{u}_{k,i}^{(m)}] \in \mathbb{R}^{d \times m}$ , which simplifies the analysis that follows. With this compact form, the gradient estimator in FedMPDD algorithm  $\hat{\mathbf{g}}_i(\mathbf{x}_k) = \frac{1}{m} \mathbf{U}_{k,i} \mathbf{U}_{k,i}^\top \mathbf{g}_i(\mathbf{x}_k)$  remains unbiased, i.e.,  $\mathbb{E}[\hat{\mathbf{g}}_i(\mathbf{x}_k)] = \frac{1}{m} \mathbb{E}[\mathbf{U}_{k,i} \mathbf{U}_{k,i}^\top] \mathbf{g}_i(\mathbf{x}_k) = \mathbf{g}_i(\mathbf{x}_k)$ , most of the derivation steps leading up to Equation (B.16) remain unchanged. Therefore, we omit those details for brevity. From (B.16) in the proof of Theorem 1, we have

$$\begin{aligned}
\mathbb{E}[\|\hat{\mathbf{g}}(\mathbf{x}_k) - \nabla f(\mathbf{x}_k)\|^2] &\leq \frac{2(1/\beta - 1)}{N(N-1)} \sum_{i=1}^N \mathbb{E}[\|\nabla f_i(\mathbf{x}_k) - \\
&\quad \nabla f(\mathbf{x}_k)\|^2] + \frac{2}{\beta N} \sum_{i \in \mathcal{A}_k} \mathbb{E}[\|\hat{\mathbf{g}}_i(\mathbf{x}_k) - \mathbf{g}_i(\mathbf{x}_k)\|^2], \\
&= \frac{2(1/\beta - 1)}{N(N-1)} \sum_{i=1}^N \mathbb{E}[\|\nabla f_i(\mathbf{x}_k) - \nabla f(\mathbf{x}_k)\|^2] \\
&\quad + \frac{2}{\beta N} \sum_{i \in \mathcal{A}_k} \mathbb{E}[\|\hat{\mathbf{g}}_i(\mathbf{x}_k)\|^2] - \mathbb{E}[\|\mathbf{g}_i(\mathbf{x}_k)\|^2], \tag{B.22}
\end{aligned}$$

the last equality holds because the estimator is unbiased and the Rademacher directions are sampled independently of all other sources of randomness. Where  $\hat{\mathbf{g}}(\mathbf{x}_k) = \frac{1}{m\beta N} \sum_{i \in \mathcal{A}_k} \mathbf{U}_{k,i} \mathbf{U}_{k,i}^\top \mathbf{g}_i(\mathbf{x}_k)$ , with  $\beta N = |\mathcal{A}_k|$  denoting the number of participating clients at round  $k$ , and  $\beta \in (0, 1]$  representing the client sampling fraction. Using JL Lemma 2 results, for  $m = \mathcal{O}(\frac{\ln(d/\delta)}{\varepsilon^2})$  into (B.22) with probability at least  $1 - \delta$ , we have

$$\begin{aligned}
\mathbb{E}[\|\hat{\mathbf{g}}(\mathbf{x}_k) - \nabla f(\mathbf{x}_k)\|^2] &\leq \frac{2(1/\beta - 1)}{N(N-1)} \sum_{i=1}^N \mathbb{E}[\|\nabla f_i(\mathbf{x}_k) - \\
&\quad \nabla f(\mathbf{x}_k)\|^2] + \frac{\epsilon(4+2\epsilon)}{\beta N} \sum_{i \in \mathcal{A}_k} \mathbb{E}[\|\mathbf{g}_i(\mathbf{x}_k)\|^2]. \tag{B.23}
\end{aligned}$$

Now, similar to the proof steps of Theorem 1 following the steps after equation (B.16) and invoking Assumption 1, we obtain the following upper bound

$$\begin{aligned}
\frac{1}{K} \sum_{k=0}^{K-1} \mathbb{E}[\|\nabla f(\mathbf{x}_k)\|^2] &\leq \frac{2}{K\eta} (f(\mathbf{x}_0) - f^*) \\
&+ \frac{2L\eta(1/\beta - 1)}{K(N-1)} \sigma^2 + \epsilon(4+2\epsilon) L\eta G^2, \tag{B.24}
\end{aligned}$$

where  $0 < \epsilon < 1$  is the distortion parameter. If we set  $\eta = \frac{1}{L\sqrt{K}}$  in (B.24), we have a convergence rate of  $\mathcal{O}(1/\sqrt{K})$  to a stationary point of  $f(\mathbf{x})$ .  $\blacksquare$

*Proof:* [Proof of Lemma 5] In the worst case where  $g_i(x^k) = g$

**TABLE VI:** Hyperparameters used for all methods on the logistic regression model.

Method	batch	lr	opt.	client participation (%)
FedSGD	1	0.01	sgd	10
QSGD	1	0.01	sgd	10
<b>FedMPDD</b>	1	0.01	sgd	10
FedSGD + Gaussian	1	0.01	sgd	10
FedSGD + Laplace	1	0.01	sgd	10

**TABLE VII:** Hyperparameters used for all methods on the CNN model from [66].

Method	batch	lr	opt.	client participation (%)
FedSGD	64	0.1	sgd	50
QSGD	64	0.1	sgd	50
<b>FedMPDD</b>	64	0.1	sgd	50
FedSGD + Laplace	64	0.1	sgd	50

is constant, each round  $k$  provides  $m$  linear equations of the form  $\langle g, u_i^{(j)} \rangle = s_i^{(j)}$  for  $j = 1, \dots, m$ . After  $T$  rounds, the adversary has  $T \times m$  linear constraints on the  $d$ -dimensional vector  $g$ . The system is underdetermined when  $T \times m < d$ , ensuring that multiple solutions exist in the  $(d - T \times m)$ -dimensional nullspace, preventing unique gradient recovery. ■

### C. Hyperparameters

This appendix summarizes the hyperparameters used for each baseline method and our proposed algorithm. To ensure reproducibility, we selected five fixed random seeds as [17, 123, 777, 2023, 424242]. Additionally, we use a separate seed, 2024, to control client data partitioning.

- **Logistic model on the MNIST dataset.** See Table VI. The best stepsize for each algorithm is selected from the set  $\{0.1, 0.01, 0.001\}$ .
- **CNN model from [66] on the MNIST and FASHIONMNIST datasets.** See Table VII. The best stepsize for each algorithm is selected from the set  $\{0.1, 0.01, 0.001\}$ .
- **CNN model from [1] on CIFAR10 dataset.** See Table VIII. The best stepsize for each algorithm is selected from the set  $\{0.01, 0.005, 0.0001\}$ .
- **LeNet model on the MNIST and FASHIONMNIST datasets.** See Table IX. The best stepsize for each algorithm is selected from the set  $\{0.1, 0.01, 0.001\}$ .

For the DLG attack hyper-parameters, we followed the procedure in [43]. To improve stability, we used the Adam optimizer for both the logistic-regression model and the CNN from [1], and the L-BFGS optimizer (history size 100, max 20 iterations) for the LeNet model and the CNN from [66].

1) **License Information for Datasets: CIFAR10.** The original CIFAR10 dataset is available under the MIT license.

**MNIST.** The original MNIST dataset is available under the CC BY-SA 3.0 license.

**FASHIONMNIST.** The original FASHIONMNIST dataset is available under the MIT license.

### D. Additional Experimental Evaluation Results

This appendix presents additional experimental results on both i.i.d. and non-i.i.d. data distributions, evaluating the proposed method in terms of communication cost reduction and privacy preservation across various datasets and models with varying dimensionalities.

Figures 4-12 provide a comprehensive comparison between the proposed FedMPDD algorithm and standard communication-efficient baselines across multiple datasets, models, and data heterogeneity settings. In particular, these figures report (i) test accuracy versus communication rounds, (ii) test accuracy versus total transmitted bits,

**TABLE VIII:** Hyperparameters used for all methods on the CNN model from [1].

Method	batch	lr	opt.	client participation (%)
FedSGD	64	0.005	sgd	100
QSGD	64	0.005	sgd	100
<b>FedMPDD</b>	64	0.005	sgd	100
FedSGD + Laplace	64	0.005	sgd	100
Top-k	64	0.005	sgd	100
lp-proj	64	0.005	sgd	100
SA-FedLora	64	0.005	sgd	100

**TABLE IX:** Hyperparameters used for all methods on the LeNet model.

Method	batch	lr	opt.	client participation (%)
FedSGD	1	0.1	sgd	50
QSGD	1	0.1	sgd	50
<b>FedMPDD</b>	1	0.1	sgd	50
FedSGD + Laplace	1	0.1	sgd	50
Top-k	1	0.1	sgd	50
lp-proj	1	0.1	sgd	50

(iii) training loss versus communication rounds, and (iv) training loss versus transmitted bits.

Figures 4 and 5 focus on the logistic regression model trained on MNIST under i.i.d. and non-i.i.d. data distributions, respectively. These results highlight that FedMPDD achieves comparable or higher accuracy than competing methods while requiring substantially fewer communicated bits. Moreover, the training loss curves demonstrate faster convergence of FedMPDD in terms of both rounds and communication cost.

Figures 6 and 9 present results for the LeNet model on FMNIST under i.i.d. and non-i.i.d. settings. Across all metrics, FedMPDD consistently improves the accuracy–communication trade-off and exhibits smoother and more stable training loss decay compared to gradient compression and noise-based baselines.

Figures 7, 8, 11, and 12 report analogous experiments for CNN models on the FMNIST and MNIST datasets. In these higher-dimensional settings, the benefits of FedMPDD become even more pronounced: the proposed method achieves similar final accuracy with significantly lower communication budgets and reaches low training loss values earlier in terms of transmitted bits. This behavior confirms that directional-derivative-based compression is particularly effective for large models.

Overall, the results in Figures 4–12 consistently demonstrate that FedMPDD offers a favorable trade-off between accuracy, convergence speed, and communication efficiency across different models, datasets, and levels of data heterogeneity.

Table X, Figure 13, and Figure 14 jointly evaluate the privacy and reconstruction behavior of the proposed FedMPDD algorithm compared to standard communication-efficient baselines under gradient inversion attacks. Table VI reports quantitative results in terms of test accuracy under a fixed communication budget, communication usage to reach a target accuracy, defendability, and reconstruction quality measured by SSIM.

As shown in Table X, classical baselines such as FedSGD, FedSGD with Gaussian or Laplace noise, and QSGD either exceed the communication budget early or remain vulnerable to gradient inversion attacks, as indicated by high SSIM values and unsuccessful defendability. In contrast, FedMPDD achieves competitive test accuracy while using significantly fewer communicated bytes and consistently maintaining successful defense against reconstruction attacks.

These observations are further supported by the qualitative reconstruction results in Figure 13. While the attacker is able to recover visually accurate digit samples for FedSGD, noise-perturbed FedSGD, and QSGD, the reconstructed images corresponding to FedMPDD appear highly noisy and uninformative, even for larger projection dimensions. This visual degradation indicates that the

transmitted directional derivatives do not reveal sufficient information for successful data recovery.

Figure 14 quantitatively summarizes the reconstruction quality using SSIM. Baseline methods exhibit high SSIM values close to one, confirming near-perfect reconstruction. In contrast, FedMPDD yields significantly lower SSIM values across all projection dimensions, demonstrating strong resistance to gradient inversion. Together, these results confirm that FedMPDD provides a favorable trade-off between accuracy, communication efficiency, and privacy preservation.

Table XI, Figure 15, and Figure 16 present a comprehensive evaluation of privacy leakage and reconstruction robustness for the LeNet model trained on the FMNIST dataset under the i.i.d. setting. The comparison includes test accuracy under a fixed communication budget, communication usage to reach a target accuracy, defendability against gradient inversion attacks, and reconstruction quality measured by SSIM.

As reported in Table XI, baseline methods such as FedSGD and QSGD either fail to provide sufficient privacy protection or incur substantially higher communication costs. While adding Laplace noise to FedSGD reduces reconstruction quality, this comes at the expense of degraded accuracy and increased communication usage.

In contrast, FedMPDD achieves significantly higher test accuracy while requiring markedly fewer transmitted bytes and consistently satisfying the defendability criterion across all tested projection dimensions.

The qualitative reconstruction results in Figure 15 further illustrate these findings. For FedSGD and QSGD, the attacker is able to recover visually meaningful input images, indicating severe privacy leakage. In comparison, the reconstructed images corresponding to FedMPDD appear highly noisy and unstructured, even for larger values of the projection dimension, demonstrating that the shared directional derivatives do not reveal sufficient information for successful data recovery.

This behavior is quantitatively confirmed by the SSIM results in Figure 16. While FedSGD and QSGD exhibit SSIM values close to one, indicating near-perfect reconstruction, FedMPDD consistently yields SSIM values close to zero. These results confirm that FedMPDD provides strong resistance to gradient inversion attacks while maintaining favorable accuracy–communication trade-offs.

Tables XIII, XIV, XV, XVI, and XVII summarize the accuracy, communication cost, and privacy behavior of different methods across non-i.i.d. data distributions and deeper CNN architectures. All results are reported under a fixed communication budget, together with the communication usage required to reach a target accuracy and the defendability against gradient inversion attacks.

Across all settings, standard baselines such as FedSGD and QSGD either fail to achieve competitive test accuracy within the communication budget or remain vulnerable to privacy leakage, as indicated by unsuccessful defendability. Adding Laplace noise to FedSGD improves privacy in some cases, but this typically comes at the expense of degraded accuracy and substantially increased communication usage.

In contrast, FedMPDD consistently achieves significantly higher test accuracy while using orders of magnitude fewer communicated bytes. This behavior is observed for both LeNet and CNN models, and persists under non-i.i.d. data distributions on MNIST and FMNIST. Moreover, FedMPDD satisfies the defendability criterion in all reported settings, demonstrating robustness to gradient inversion attacks without relying on explicit noise injection.

Notably, as the projection dimension increases, FedMPDD exhibits a smooth accuracy–communication trade-off: larger projection dimensions improve accuracy at the cost of increased communication, while still maintaining strong privacy guarantees. These results confirm that FedMPDD scales favorably to deeper models and heterogeneous data while simultaneously addressing communication efficiency and privacy preservation.

Table XII, Figure 17, and Figure 18 evaluate the privacy leakage and reconstruction robustness of different communication-efficient methods for the CNN model on the MNIST dataset under the i.i.d.

setting. The comparison includes test accuracy under a fixed communication budget, communication usage to reach a target accuracy, defendability against gradient inversion attacks, and reconstruction quality measured by SSIM.

As shown in Table XII, baseline methods such as FedSGD and QSGD either exhibit poor test accuracy under the fixed communication budget or remain vulnerable to gradient inversion attacks, as reflected by high SSIM values and unsuccessful defendability. Adding Laplace noise to FedSGD reduces reconstruction quality but requires substantially higher communication usage and still fails to achieve a favorable accuracy–communication trade-off. In contrast, FedMPDD achieves significantly higher test accuracy while using orders of magnitude fewer transmitted bytes and consistently satisfying the defendability criterion across all tested projection dimensions.

The qualitative reconstruction results in Figure 17 further support these findings. For FedSGD, noise-perturbed FedSGD, and QSGD, the attacker is able to recover visually meaningful digit structures, indicating severe privacy leakage. In comparison, the reconstructed images corresponding to FedMPDD are highly distorted and lack semantic structure, demonstrating that the compressed directional information is insufficient for successful input recovery.

Finally, Figure 18 reports SSIM as a function of attack iteration. Baseline methods rapidly converge to high SSIM values, indicating increasingly accurate reconstructions as the attack progresses. In contrast, FedMPDD consistently maintains low SSIM values across iterations, confirming sustained resistance to gradient inversion attacks throughout the optimization process. Together, these results demonstrate that FedMPDD provides strong privacy protection while preserving favorable accuracy and communication efficiency for CNN models.

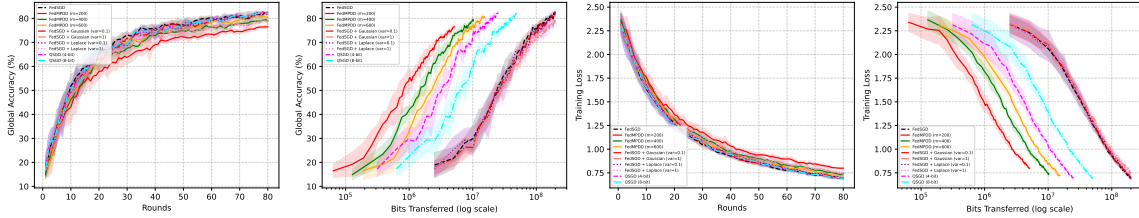
Figure 19 illustrates the evolution of reconstruction quality over training epochs for the LeNet model under a gradient inversion attack. Specifically, the figure reports the SSIM values produced by the attack in [63] when applied to the projected directional derivative estimator used in FedMPDD with projection dimension  $m = 600$ . Across all training epochs, the SSIM values remain consistently low and do not exhibit any increasing trend, indicating that the attacker is unable to recover meaningful information about the private inputs as training progresses. This result demonstrates that FedMPDD enforces a stable and persistent privacy guarantee throughout the entire training process, rather than relying on privacy that degrades over time.

Table XVIII illustrates the impact of the number of random directions  $m$  on the test accuracy of FedMPDD for the LeNet model on MNIST. As predicted in Remark 1, increasing  $m$  improves accuracy by reducing the distortion introduced by JL Lemma. Specifically, smaller values of  $m$  lead to higher projection error and consequently degraded optimization performance, while larger values of  $m$  yield progressively better accuracy as the projected directional derivative more faithfully preserves gradient information.

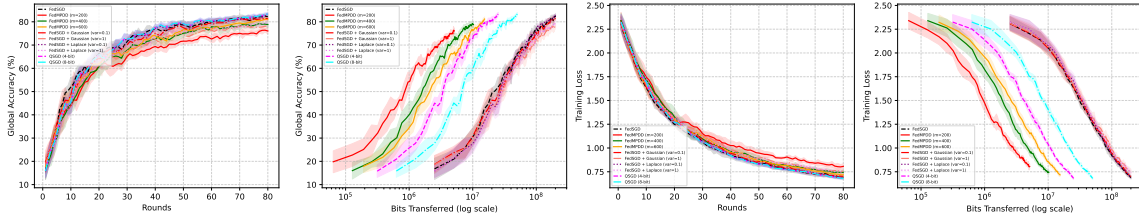
Importantly, the observed accuracy gains saturate as  $m$  increases, indicating a clear communication–accuracy trade-off. This behavior is consistent with the JL embedding guarantee, where choosing  $m$  within the theoretically valid regime is sufficient to control the distortion parameter  $\epsilon$  and ensure stable convergence. These results confirm that selecting  $m$  according to the JL scaling in Remark 1 yields both strong empirical performance and adherence to the theoretical guarantees.

Table XIX reports the average per-round, per-client latency required to compute the directional derivative encodings in FedMPDD for different numbers of random directions  $m$  on the LeNet–MNIST setup. As shown, even for larger values of  $m$ , the measured client-side computation time remains on the order of milliseconds, confirming that the encoding step does not constitute a computational bottleneck in practice. These empirical results are consistent with Remark 2. Although the theoretical encoding cost of FedMPDD scales as  $\mathcal{O}(dm)$ , this cost is negligible relative to the overall training pipeline in our experiments. Moreover, as discussed in Remark 2, the directional derivative computation can be efficiently implemented using Jacobian–vector products, avoiding explicit full-

gradient computation. This projected-forward strategy further reduces practical overhead and can even lead to computational savings in deep models, making FedMPDD well suited for resource-constrained client devices.



**Fig. 4:** Training loss and accuracy curves versus communication rounds and number of transmitted bits for the logistic model on the MNIST dataset (i.i.d.).



**Fig. 5:** Training loss and accuracy curves versus communication rounds and number of transmitted bits for the logistic model on the MNIST dataset (non-i.i.d.).

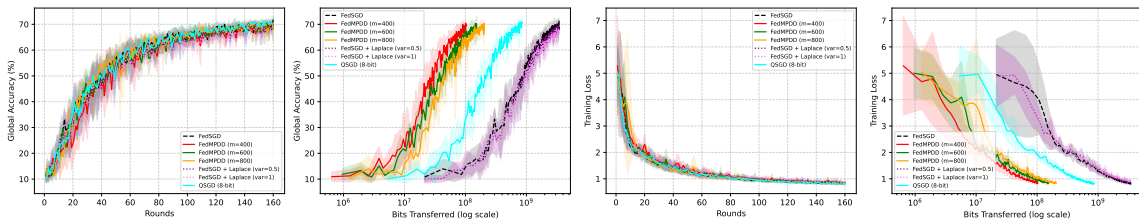


**Fig. 6:** Training loss and accuracy curves versus communication rounds and number of transmitted bits for the LeNet model on the FMNIST dataset (i.i.d.).

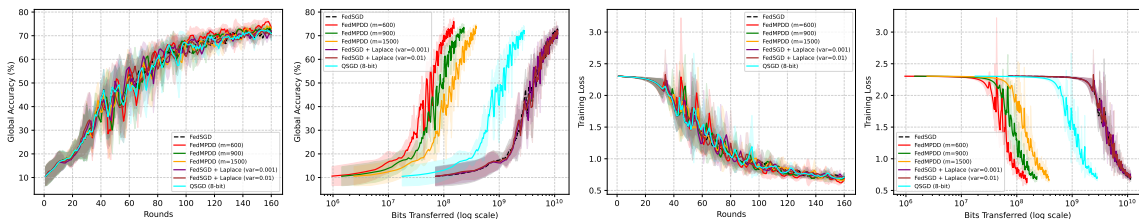


**Fig. 7:** Training loss and accuracy curves versus communication rounds and number of transmitted bits for the CNN model from [66] on the FMNIST dataset (i.i.d.).

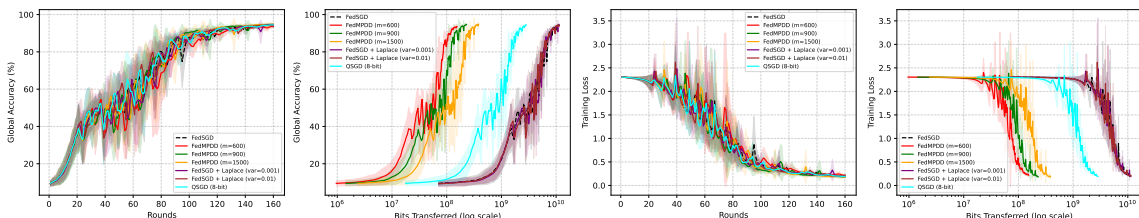


**Fig. 8:** Training loss and accuracy curves versus communication rounds and number of transmitted bits for the CNN model from [66] on the MNIST dataset (i.i.d.).

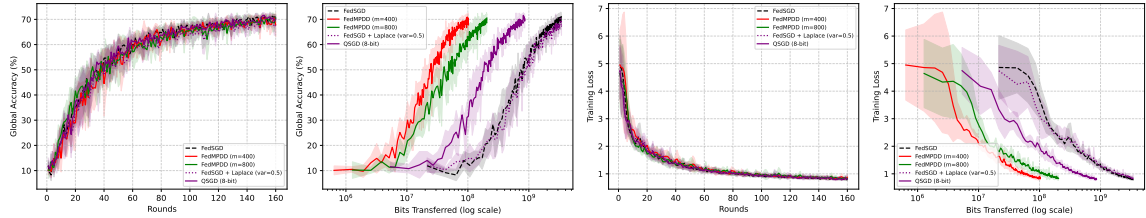


**Fig. 9:** Training loss and accuracy curves versus communication rounds and number of transmitted bits for the LeNet model on the FMNIST dataset (non-i.i.d.).

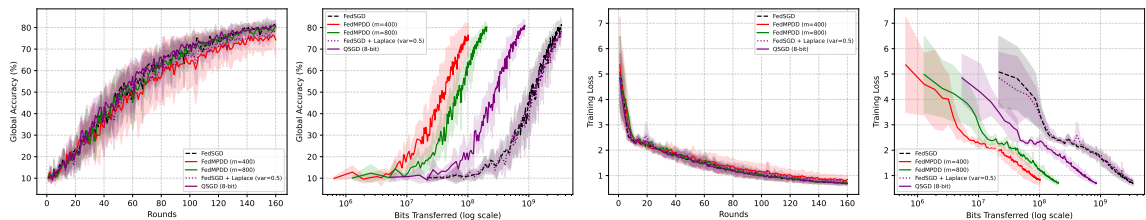


**Fig. 10:** Training loss and accuracy curves versus communication rounds and number of transmitted bits for the LeNet model on the MNIST dataset (non-i.i.d.).

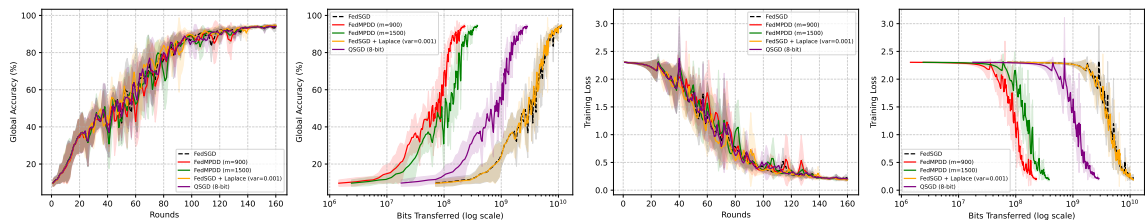


**Fig. 11:** Training loss and accuracy curves versus communication rounds and number of transmitted bits for the CNN model from [66] on the MNIST dataset (non-i.i.d.).

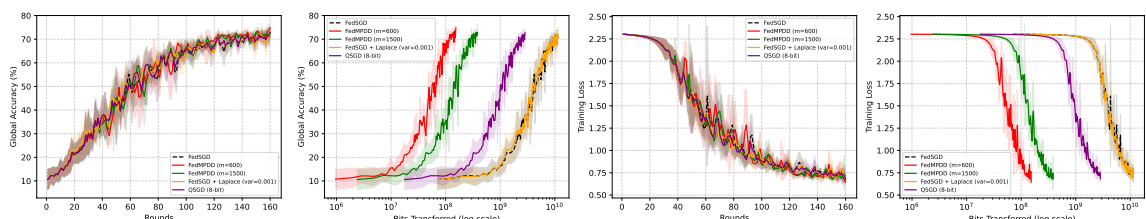


**Fig. 12:** Training loss and accuracy curves versus communication rounds and number of transmitted bits for the CNN model from [66] on the FMNIST dataset (non-i.i.d.).

**TABLE X:** Comparison of test accuracy under a fixed communication budget, communication usage for target accuracy, privacy leakage, and reconstruction quality on MNIST (i.i.d.) using the attack of [43] with a logistic model. A  $\star$  in the Test Acc column indicates that the communication budget was already exceeded in the first iteration of the algorithm.

Method	Bytes Budget	Test Acc	Target Acc	Used Bytes	Defendability	SSIM
FedSGD	2000000	$\star$	60	40192000.0	$\times$	1.00
FedSGD + Gaussian (var=0.1)	2000000	$\star$	60	42704000.0	$\times$	0.80
FedSGD + Gaussian (var=1)	2000000	$\star$	60	45216000.0	$\times$	0.59
FedSGD + Laplace (var=0.1)	2000000	$\star$	60	42704000.0	$\times$	0.82
FedSGD + Laplace (var=1)	2000000	$\star$	60	45216000.0	$\times$	0.60
<b>FedMPDD (m=200)</b>	2000000	<b>65.29</b>	60	<b>1536000.0</b>	$\checkmark$	0.03
<b>FedMPDD (m=400)</b>	2000000	<b>57.62</b>	60	<b>2432000.0</b>	$\checkmark$	0.14
<b>FedMPDD (m=600)</b>	2000000	<b>48.85</b>	60	<b>3456000.0</b>	$\checkmark$	0.13
QSGD (4-bit)	2000000	38.92	60	5343440.0	$\times$	0.88
QSGD (8-bit)	2000000	28.86	60	10681440.0	$\times$	0.99

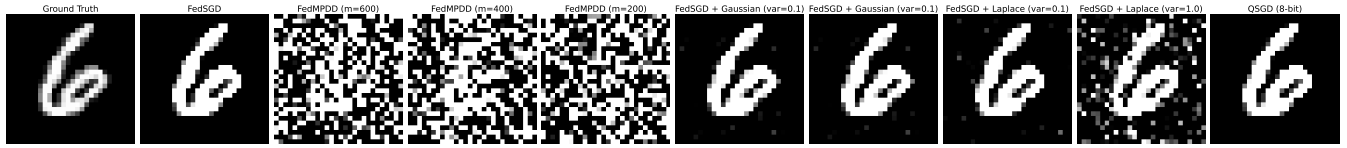


**Fig. 13:** Attack results on logistic model using MNIST dataset.

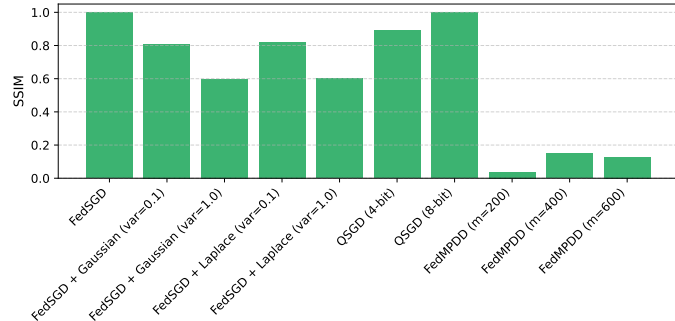


**Fig. 14:** SSIM bar plot on logistic model using MNIST dataset.

**TABLE XI:** Comparison of test accuracy under a fixed communication budget, communication usage for target accuracy, privacy leakage, and reconstruction quality on FMNIST (i.i.d.) using the attack of [43] with LeNet model.

Method	Bytes Budget	Test Acc	Target Acc	Used Bytes	Defendability	SSIM
FedSGD	90000000	15.85	60	1331859200.0	✗	1.00
FedSGD + Laplace (var=0.5)	90000000	15.76	60	1245932800.0	✓	$\ll 0.03$
FedSGD + Laplace (var=1)	90000000	15.91	60	1525193600.0	✓	$\ll 0.03$
<b>FedMPDD (m=400)</b>	90000000	<b>66.77</b>	60	<b>44160000.0</b>	✓	$\ll 0.03$
<b>FedMPDD (m=600)</b>	90000000	<b>66.10</b>	60	<b>61440000.0</b>	✓	$\ll 0.03$
<b>FedMPDD (m=800)</b>	90000000	<b>64.84</b>	60	<b>78080000.0</b>	✓	$\ll 0.03$
QSGD (8-bit)	90000000	25.73	60	311576000.0	✗	0.99



**Fig. 15:** Attack results on LeNet using FMNIST dataset.

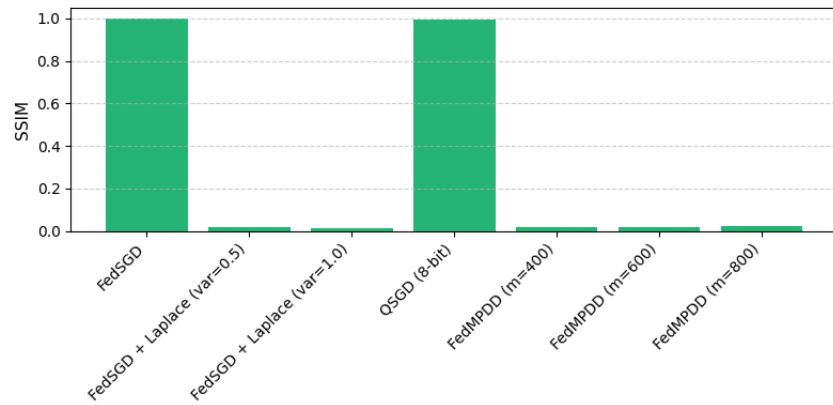


**Fig. 16:** SSIM bar plot on LeNet using FMNIST dataset.

**TABLE XII:** Comparison of test accuracy under a fixed communication budget, communication usage for target accuracy, privacy leakage, and reconstruction quality on MNIST (i.i.d.) using the attack of [63] with CNN model from [66].

Method	Bytes Budget	Test Acc	Target Acc	Used Bytes	Defendability	SSIM
FedSGD	150000000	10.40	60	3980569600.0	✗	0.81
FedSGD + Laplace (var=0.001)	150000000	10.30	60	4193814400.0	✗	0.48
FedSGD + Laplace (var=0.01)	150000000	10.33	60	3625161600.0	✓	0.13
<b>FedMPDD (m=600)</b>	150000000	<b>93.26</b>	60	<b>64320000.0</b>	✓	0.17
<b>FedMPDD (m=900)</b>	150000000	<b>91.46</b>	60	<b>86400000.0</b>	✓	0.28
<b>FedMPDD (m=1500)</b>	150000000	<b>59.46</b>	60	<b>146400000.0</b>	✓	0.28
QSGD (8-bit)	150000000	14.56	60	977460000.0	✗	0.64

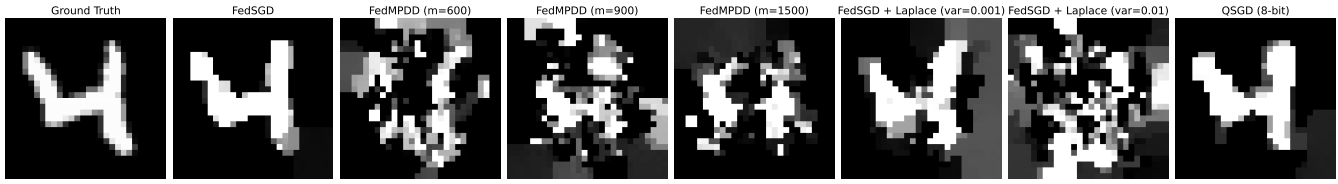


**Fig. 17:** Attack results on CNN model from [66] using MNIST dataset.

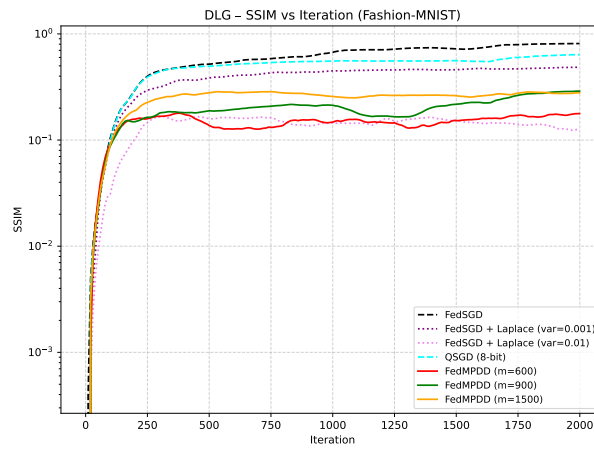


**Fig. 18:** SSIM plot versus iteration on CNN model from [66] using MNIST dataset.

**TABLE XIII:** Comparison of test accuracy under a fixed communication budget, communication usage for target accuracy, and privacy leakage on MNIST (non-i.i.d.) using the attack of [63] with LeNet model.

Method	Bytes Budget	Test Acc	Target Acc	Used Bytes	Defendability
FedSGD	90000000	11.06	60	1460748800.0	✗
FedSGD + Laplace (var=0.5)	90000000	12.75	60	1482230400.0	✓
<b>FedMPDD (m=400)</b>	90000000	<b>76.00</b>	60	<b>51840000.0</b>	✓
<b>FedMPDD (m=800)</b>	90000000	<b>57.80</b>	60	<b>93440000.0</b>	✓
QSGD (8-bit)	90000000	18.66	60	359924000.0	✗

**TABLE XIV:** Comparison of test accuracy under a fixed communication budget, communication usage for target accuracy, and privacy leakage on FMNIST (non-i.i.d.) using the attack of [43] with LeNet model.

Method	Bytes Budget	Test Acc	Target Acc	Used Bytes	Defendability
FedSGD	90000000	12.05	60	1288896000.0	✗
FedSGD + Laplace (var=0.5)	90000000	15.06	60	1224451200.0	✓
<b>FedMPDD (m=400)</b>	90000000	<b>69.47</b>	60	<b>37760000.0</b>	✓
<b>FedMPDD (m=800)</b>	90000000	<b>61.18</b>	60	<b>74240000.0</b>	✓
QSGD (8-bit)	90000000	24.30	60	306204000.0	✗

**TABLE XV:** Comparison of test accuracy under a fixed communication budget, communication usage for target accuracy, privacy leakage, and reconstruction quality on FMNIST (i.i.d.) using the attack of [63] with CNN model from [66].

Method	Bytes Budget	Test Acc	Target Acc	Used Bytes	Defendability
FedSGD	150000000	11.74	60	5757609600.0	✗
FedSGD + Laplace (var=0.001)	150000000	11.95	60	4975712000.0	✓
FedSGD + Laplace (var=0.01)	150000000	12.48	60	5402201600.0	✓
<b>FedMPDD (m=600)</b>	150000000	<b>75.81</b>	60	<b>73920000.0</b>	✓
<b>FedMPDD (m=900)</b>	150000000	<b>62.36</b>	60	<b>103680000.0</b>	✓
<b>FedMPDD (m=1500)</b>	150000000	<b>47.32</b>	60	<b>199200000.0</b>	✓
QSGD (8-bit)	150000000	15.51	60	1421760000.0	✗

**TABLE XVI:** Comparison of test accuracy under a fixed communication budget, communication usage for target accuracy, and privacy leakage on MNIST (non-i.i.d.) using the attack of [43] with CNN model from [66].

Method	Bytes Budget	Test Acc	Target Acc	Used Bytes	Defendability
FedSGD	200000000	11.40	60	3696243200.0	✗
FedSGD + Laplace (var=0.001)	200000000	11.04	60	3696243200.0	✗
<b>FedMPDD (m=900)</b>	200000000	<b>93.08</b>	60	<b>90720000.0</b>	✓
<b>FedMPDD (m=1500)</b>	200000000	<b>80.67</b>	60	<b>151200000.0</b>	✓
QSGD (8-bit)	200000000	21.84	60	1030776000.0	✗

**TABLE XVII:** Comparison of test accuracy under a fixed communication budget, communication usage for target accuracy, privacy leakage, and reconstruction quality on FMNIST (non-i.i.d.) using the attack of [43] with CNN model from [66].

Method	Bytes Budget	Test Acc	Target Acc	Used Bytes	Defendability
FedSGD	150000000	12.22	60	5828691200.0	✗
FedSGD + Laplace (var=0.001)	150000000	12.03	60	5615446400.0	✓
<b>FedMPDD (m=600)</b>	150000000	<b>70.83</b>	60	<b>74880000.0</b>	✓
<b>FedMPDD (m=1500)</b>	150000000	<b>51.32</b>	60	<b>199200000.0</b>	✓
QSGD (8-bit)	150000000	13.51	60	1457304000.0	✗

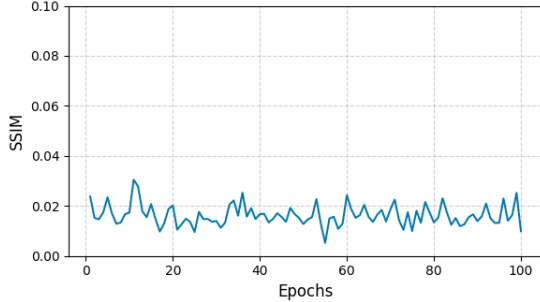


**Fig. 19:** The SSIM scores produced by the attack in [63] on the LeNet model using the *projected directional derivative* estimator  $\hat{\mathbf{g}}_i(\mathbf{x})$  with  $m = 600$  in FedMPDD remain uniformly low over 100 training epochs, confirming that FedMPDD enforces a constant privacy guarantee throughout the entire training process.

**TABLE XVIII:** FedMPDD performance with varying numbers of random directions  $m$  on the MNIST dataset using the LeNet model.

Method	Test Acc. (%)
FedMPDD (m=50)	30.44
FedMPDD (m=200)	75.02
FedMPDD (m=400)	77.52
FedMPDD (m=600)	79.02

**TABLE XIX:** Per-round, per-client latency (ms) to compute  $\mathbf{s}_i^k[j] = (\mathbf{u}_{k,i}^{(j)})^\top \mathbf{g}_i(\mathbf{x}_k)$ , averaged over clients and rounds on LeNet–MNIST.

# random directions $m$	Avg. latency (ms)
400	0.43
600	0.61
800	0.93